Quarterly Reviews of Biophysics **40**, 1 (2007), pp. 1–53. © 2007 Cambridge University Press
doi:10.1017/S003358350700460X Printed in the United Kingdom
First published online 13 June 2007

Long-range distance determinations in biomacromolecules by EPR spectroscopy

Olav Schiemann* and Thomas F. Prisner*

Institute of Physical and Theoretical Chemistry, Center for Biomolecular Magnetic Resonance, J. W. Goethe-University Frankfurt, 60438 Frankfurt am Main, Germany

Abstract. Electron paramagnetic resonance (EPR) spectroscopy provides a variety of tools to study structures and structural changes of large biomolecules or complexes thereof. In order to unravel secondary structure elements, domain arrangements or complex formation, continuous wave and pulsed EPR methods capable of measuring the magnetic dipole coupling between two unpaired electrons can be used to obtain long-range distance constraints on the nanometer scale. Such methods yield reliably and precisely distances of up to 80 Å, can be applied to biomolecules in aqueous buffer solutions or membranes, and are not size limited. They can be applied either at cryogenic or physiological temperatures and down to amounts of a few nanomoles. Spin centers may be metal ions, metal clusters, cofactor radicals, amino acid radicals, or spin labels. In this review, we discuss the advantages and limitations of the different EPR spectroscopic methods, briefly describe their theoretical background, and summarize important biological applications. The main focus of this article will be on pulsed EPR methods like pulsed electron–electron double resonance (PELDOR) and their applications to spin-labeled biosystems.

* Correspondence may be addressed to either author at: Institute of Physical and Theoretical Chemistry, Center for Biomolecular Magnetic Resonance, J. W. Goethe-University, Max-von-Laue-Str. 7, 60438 Frankfurt am Main, Germany.
Tel.: +49 (0) 69 798 29 786; Fax: +49 (0) 69 798 29 404.
E-mail: O. Schiemann (o.schiemann@epr.uni-frankfurt.de); T. F. Prisner (prisner@chemie.uni-frankfurt.de)

1. Introduction

One of the major topics in biomolecular research is the mechanistic understanding of biological functions on a molecular level, which is commonly approached by studying reaction kinetics, structures, and structural dynamics. With respect to structure, X-ray diffraction allowed to solve the structure of biomolecular complexes like the plant photosystem II (PS II) (Loll *et al.* 2005), the transcription complex (Cramer *et al.* 2001; Gnatt *et al.* 2001), and the ribosome (Tocilj *et al.* 1999; Ban *et al.* 2000; Nissen *et al.* 2000; Yusupov *et al.* 2001) with high resolution. However, the structures obtained are those of biosystems in the solid state of the crystal. In contrast, nuclear magnetic resonance (NMR) spectroscopy can be performed on biomolecules in liquid solution and additionally yields structural and dynamical information (Wüthrich, 1986; Ernst, 1992; Bonvin *et al.* 2005). Yet, high-resolution liquid-state NMR spectroscopy is currently restricted to biological systems with a size below $\sim$50 kDa. Thus, to be able to study structures, folding, and conformational changes of large biomolecules in solution, other biophysical spectroscopic methods are required, for example fluorescence (Lakowicz, 2006) and electron paramagnetic resonance (EPR) spectroscopy (Hoff, 1989; Schweiger & Jeschke, 2001). Especially, fluorescence resonance energy transfer (FRET) and certain EPR-based experiments are suited to measure large distances in the nanometer range without restriction to the size of the biomolecule. Collecting several of these long-range constraints can yield global structure elements, information about domain arrangements, complex formation, and structural changes upon ligand binding. Combined with molecular dynamics (MD) simulations this approach is extremely valuable (Sale *et al.* 2004).

Continuous wave EPR methods were already applied to biological systems in the 1960s and 1970s (Berliner, 1976), but were mainly complicated by unspecific labeling methods and the inhomogeneous continuous wave EPR line widths, which limited measurements to distances below 20 Å. Three important advances raised these limits dramatically: (1) the invention of site-directed spin labeling (Altenbach *et al.* 1990; Berliner, 1998), (2) the technical development of EPR spectrometers at high fields/high frequencies (Bennati & Prisner, 2005; Möbius *et al.* 2005), and (3) the methodological development of pulse sequences suitable for biological applications (Prisner *et al.* 2001; Calle *et al.* 2006). Consequently, EPR spectroscopy has become a growing field in biomolecular sciences.

Here, we first give a short overview of EPR methods suitable to measure long-range distances and then summarize examples of their application to biological systems. Pulsed EPR methods applied to spin-labeled biomacromolecules and complexes thereof are the main focus of this review. Other general reviews related to this area of research are Berliner *et al.* (2000), Lakshmi & Brudvig (2001) and Eaton & Eaton (2004). More specific reviews will be mentioned in the respective sections.

2. Methods and theory

2.1 Magnetic dipole–dipole interaction

Distance determination relies in all EPR methods on the magnetic dipole–dipole interaction between the magnetic moments $\vec{\mu}_A$ and $\vec{\mu}_B$ of two spins A and B. Both spins can either be electron spins (dipolar spectroscopy) or one of them can be a nuclear spin (hyperfine

spectroscopy). The former case is considered here. The interaction energy E between the two magnetic moments is given by

$$E = \frac{\vec{\mu}_A \cdot \vec{\mu}_B}{R^3} - \frac{3\,(\vec{\mu}_A \cdot \vec{R})\,(\vec{\mu}_B \cdot \vec{R})}{R^5}, \tag{1}$$

where R is the distance between A and B. This classical energy expression can be converted to a quantum mechanical spin Hamiltonian using the relation between the magnetic moment of the electron and the electron spin operator $\vec{S} = (S_x, S_y, S_z)$

$$\vec{\mu} = -\gamma_e \hbar \vec{S}, \tag{2}$$

where γ_e is the magnetogyric ratio of the electron and $\hbar$ is the Planck constant divided by 2π. This dipolar Hamiltonian H_{dip} is usually written in the following way (Slichter, 1980)

$$H_{dip} = \frac{g^A\, g^B\, \beta_e^2}{R^3}(A + B + C + D + E + F) \tag{3}$$

with g defined as the g-value of radial A and B and β_e as the Bohr magneton. The terms A–F represent products of spin operators and angular expressions in spherical coordinates θ, φ, and R describing the orientation of the molecule with respect to the external magnetic field:

$$\left.\begin{aligned}
A &= S_z^A S_z^B (1 - 3\cos^2\theta)\\
B &= -\tfrac{1}{4}(S_+^A S_-^B + S_-^A S_+^B)(1 - 3\cos^2\theta)\\
C &= -\tfrac{3}{2}(S_+^A S_z^B + S_z^A S_+^B)\sin\theta\,\cos\theta\cdot e^{-i\varphi}\\
D &= -\tfrac{3}{2}(S_-^A S_z^B + S_z^A S_-^B)\sin\theta\,\cos\theta\cdot e^{i\varphi}\\
E &= -\tfrac{3}{4} S_+^A S_+^B \sin^2\theta\cdot e^{-2i\varphi}\\
F &= -\tfrac{3}{4} S_-^A S_-^B \sin^2\theta\cdot e^{2i\varphi}.
\end{aligned}\right\} \tag{4}$$

If the dipolar coupling is small compared to the Zeeman splitting of the electron spin states and the g-values are only weakly anisotropic, the dipolar splitting of the EPR transitions is mainly determined by the secular term A. In this case, the dipolar frequency is given by

$$\omega_{dip} = \frac{D_{dip}}{R^3}(1 - 3\cos^2\theta) \tag{5}$$

with the splitting constant D_{dip} calculated to $2\pi \times 52\ \mathrm{MHz/nm^3}$, with $g^A = g^B = 2$. As can be seen from Eq. (5), ω_{dip} varies from $-2D_{dip}/R^3$ to $+1D_{dip}/R^3$ for a rotation of the dipolar axis R parallel ($\theta = 0^\circ$) to perpendicular ($\theta = 90^\circ$) with respect to the external magnetic field B_0. As can also be infered from Eq. (5), the average value of the dipolar interaction is zero for randomly orientated molecules and the dipolar interaction vanishes at the so-called magic angle ($\theta = 54{\cdot}7^\circ$). Therefore, the dipolar interaction is averaged to zero for molecules rotating fast compared to the inverse coupling strength. Differently, the spectra of slowly rotating molecules or of frozen samples are a superposition of spectra of the randomly oriented biradicals, each consisting of two lines splitted by the dipolar coupling. The resulting spectrum of such a sample of randomly oriented molecules is called Pake pattern (see Fig. 1). The edge-to-edge distance of the Pake pattern corresponds to the dipolar splitting for molecules with an angle of $\theta = 0^\circ$; the peak-to-peak distance corresponds to the dipolar splitting for molecules with

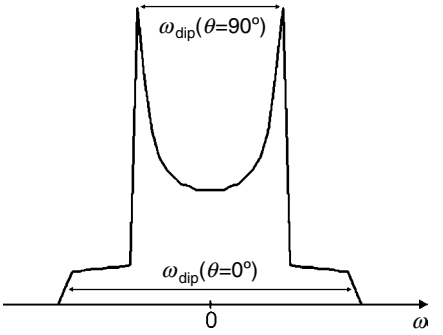

Fig. 1. Pake pattern with peaks at $\pm\frac{1}{2}\omega_{dip}$ and edges at $\pm\omega_{dip}$ corresponding to $\theta=90^\circ$ and 0°, respectively. The splitting between the two peaks is $\omega_{dip}(\theta=90^\circ)$ and the splitting between the two edges is $\omega_{dip}(\theta=0^\circ)=2\omega_{dip}(\theta=90^\circ)$. In the case of pulsed EPR experiments like PELDOR, DQC, and '2+1' the peaks appear at $\pm\omega_{dip}$ and the edges at $\pm2\omega_{dip}$.

$\theta=90^\circ$. These two peaks are usually the most easily observeable features in spectra of such samples.

For distances shorter than 1 nm or in the case of conjugated bridges between the two radicals, also the exchange interaction J has to be taken into account. If this interaction is not orientation-dependent, it will only shift peak-to-peak and edge-to-edge distances by $+2\pi J$. Given that the full Pake powder pattern can be observed with sufficient accuracy, both quantities R and J can be determined independently (Weber *et al.* 2002). For very short distances, where the splitting by dipolar and exchange coupling exceeds the difference in Larmor frequencies of spins A and B, the situation becomes more complicated.

Different EPR methods have been developed to reveal the dipolar interaction, depending on the spectral and dynamical properties of the paramagnetic centers, as well as the distance R between them. In the following sections, we will briefly describe these different methods, their application range, and limitations.

2.2 Continuous wave EPR

For paramagnetic centers with distances below 2 nm the dipolar splitting can be observed directly by continuous wave EPR spectroscopy (Hustedt *et al.* 1997, 2006), provided the intrinsic linewidth of at least one of the paramagnetic centers involved is smaller than the dipolar coupling. Therefore, it has been most successfully applied to organic radicals and half-integer spin transition metal ions.

Usually, the dipolar splitting is smaller than the intrinsic linewidth and leads only to a line broadening in biological samples. In these cases, deconvolution methods have to be used to disentangle the dipolar contribution to the linewidth from other contributions (Berliner *et al.* 2000). However, such methods require that the intrinsic linewidth of the paramagnetic center has to be measured without dipolar coupling under otherwise identical conditions, which is not always possible. In addition, from the continuous wave EPR spectrum itself it is impossible to distinguish static dipolar broadening from dipolar relaxation broadening (see Section 2.6) and at short distances, the exchange interaction might contribute to the splitting, which may both easily lead to wrong distances. Numerically, the deconvolution method is not very stable for spectra with unresolved dipolar peaks and needs high signal-to-noise ratios to avoid artifacts

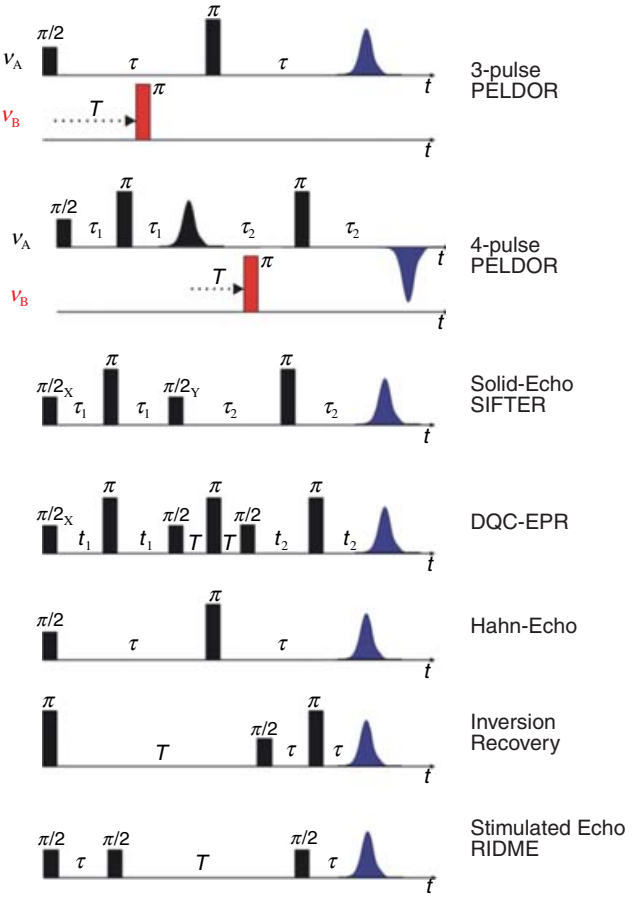

Fig. 2. Pulse sequences as discussed in the article.

(see discussion in Section 2.3.1.3). Therefore, although the method has been shown to yield quantitative distances in the range of 1–2 nm, it is commonly applied in a more qualitative fashion for distance determination between close paramagnetic centers. The advantage of this method is its easy experimental accessibility and the possibility to measure at physiological temperatures.

2.3 Pulsed electron–electron dipolar spectroscopy

2.3.1 PELDOR

At low temperatures in disordered powder samples of paramagnetic centers with a spin of $S=\frac{1}{2}$, the linewidth is dominated by inhomogeneous broadening caused by unresolved hyperfine couplings to nearby nuclei and the anisotropy of the g tensor. In such cases, pulsed experiments, like the Hahn-echo sequence (see Fig. 2), can be performed to refocus all static inhomogeneous contributions and to recover the much narrower homogeneous linewidth, given by the transversal relaxation rate $1/T_2$, thus tremendously increasing spectral resolution. This allows extension of the measurable distance R between two paramagnetic centers from 2 nm up to a limit,

where the dipolar splitting becomes comparable to the homogeneous linewidth. A pulsed EPR method capable of recovering dipolar couplings is called pulsed electron–electron double resonance (PELDOR) (Milov *et al.* 1981, 1984) or sometimes also named double electron–electron resonance (DEER) (Larsen & Singel, 1993). The three-pulse version of PELDOR (see Fig. 2) is identical to Hahn's spin echo double resonance (SEDOR) sequence used to detect the coupling between two nuclear spins (Mehring & Weberruß, 2001). In PELDOR, a two-pulse Hahn echo sequence with a fixed pulse separation time τ is employed to selectively monitor the echo intensity $V(T)$ of the paramagnetic species A of the A–B spin pair. An additional microwave pulse at time T and with a frequency resonant with spin B selectively flips this spin B. This stimulated spin-flip induces a sudden change in the Larmor frequency of spin A by $\pm\omega_{\mathrm{dip}}$, so that the A spins precess with this altered frequency in the transversal plane, which leads to a non-perfect refocusing of the A spins at the echo time 2τ. By variation of the time position T of the inversion pulse, the dephasing angle can be changed to induce a periodic modulation of the A-spin echo intensity:

$$V(T) = V_0 \cos(\omega_{\mathrm{dip}} \cdot T), \tag{6}$$

where ω_{dip} is the dipolar coupling frequency [see Eq. (5)] and V_0 is the echo intensity at $T=0$ (Milov *et al.* 1998). The modulation depth is 200% (full inversion of the echo signal) in an ideal case, where spins A and B are spectrally well-separated and both are ideally excited by the detection and inversion pulses, respectively. In most biological applications, the paramagnetic species A and B are identical nitroxide radicals. Spins A and B are then defined by their spectral position in the EPR spectra. At X-band frequencies, the spectrum of a nitroxide radical is dominated by the strong anisotropic hyperfine coupling of the ^{14}N nucleus with a nuclear spin of $I=1$. This leads to a three-line spectrum with a hyperfine splitting of about 100 MHz, if the molecular plane is perpendicular to the magnetic field (molecular z axis parallel to B_0) and is only 10 MHz for all magnetic field orientations in the plane (see Fig. 3). In a PELDOR experiment, the spins A and B are usually chosen as those with a resonance frequency corresponding to the low-field wing and to the center of the nitroxide spectrum, respectively (see Fig. 4*b*). This choice defines the A spins as molecules in the nitrogen nuclear spin state $m_{\mathrm{I}} = -1$ and with the molecular z axis almost parallel to B_0, while the B spin ensemble consists of all molecules in the $m_{\mathrm{I}} = 0$ state and molecules in the $m_{\mathrm{I}} = \pm 1$ state with the molecular z axis perpendicular to B_0. The excitation bandwidths of inversion and detection pulses have to be chosen small enough to avoid spectral overlap. On the other hand, the excitation width of the inversion pulse should be as large as possible to achieve a deep modulation. The fraction of spins B excited by the inversion pulse is described by the modulation depth parameter λ:

$$V(T) = V_0(1-\lambda+\lambda \cdot \cos(\omega_{\mathrm{dip}} \cdot T)). \tag{7}$$

If the two nitroxides in the biradical are flexible, the orientation between their molecular z axis z_{A} and z_{B} and the R vector will be almost randomly distributed. In such cases, the modulation depth parameter λ may be approximated to be independent of the orientation of the biradical with respect to the external magnetic field. Therefore, $V(T)$ can be readily integrated over all orientations:

$$V(T) = V_0\left(1-\lambda+\lambda\int_0^{\pi/2} \cos\left(\frac{D_{\mathrm{dip}}}{R^3}(1-3\cos^2\theta)\,T\right)\sin\theta\,\mathrm{d}\theta\right). \tag{8}$$

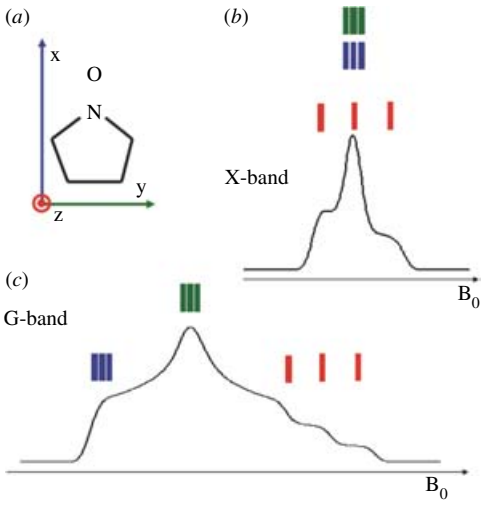

Fig. 3. Nitroxide EPR spectra. (*a*) Axis system within a nitroxide. The *g*- and *A*-axes systems are considered to be collinear. (*b*) Typical field-sweep spectrum of a nitroxide in frozen solution, acquired at X-band (9·6 GHz). The spectrum is dominated by the large hyperfine splitting of A_{zz} (red lines). The two other hyperfine splittings corresponding to A_{xx} (blue lines) and A_{yy} (green lines) are hidden under the inhomogeneous linewidth of the central peak. The *g*-anisotropy is not resolved. (*c*) The same nitroxide at G-band (180 GHz). This spectrum is dominated by the *g*-anisotropy of the nitroxide. g_{xx}, g_{yy}, and g_{zz} are clearly separated. The hyperfine splitting of A_{zz} can be seen on g_{zz}, the hyperfine splittings on g_{xx} and g_{yy} are not resolved.

Under such conditions, the time domain signal is the sum of an inverse Fourier transform of a Pake pattern in frequency space and a constant offset with amplitude $V_0(1-\lambda)$. Note that the splitting of the corresponding frequency spectrum is twice as large as in the original Pake pattern observed by continuous wave EPR experiments. The time domain signal is characterized by a fast initial decay and a fast damping of the dipolar oscillations due to interference of the θ-distributed oscillation frequencies from the Pake pattern (see Fig. 4*c*) and an offset given by

$$V(T\rightarrow\infty)=V_0(1-\lambda). \tag{9}$$

2.3.1.1 Multi-spin clusters

If N identical spins are coupled in a cluster, the total signal can be described as a sum of the products of individual two-spin interactions between spins K and J (Milov *et al.* 1984):

$$V(T)=\frac{V_0}{N}\sum_{K=1}^{N}\prod_{\substack{J=1\\J\neq K}}^{N}\left(1-\lambda+\lambda\int_0^{\pi/2}\cos\left(\frac{D_{\mathrm{dip}}}{R_{JK}^3}(1-3\cos^2\theta)\;T\right)\sin\theta\;\mathrm{d}\theta\right). \tag{10}$$

The echo amplitude $V(T)$ levels for $T\rightarrow\infty$ at

$$V(T\rightarrow\infty)=V_0(1-\lambda)^{N-1}. \tag{11}$$

Thus, the number of spins N in the cluster can be determined from the signal amplitude at large values of T, if the parameter λ is known independently from a structurally similar biradical system, as shown recently in a PELDOR study on a series of model systems (Bode *et al.* 2007).

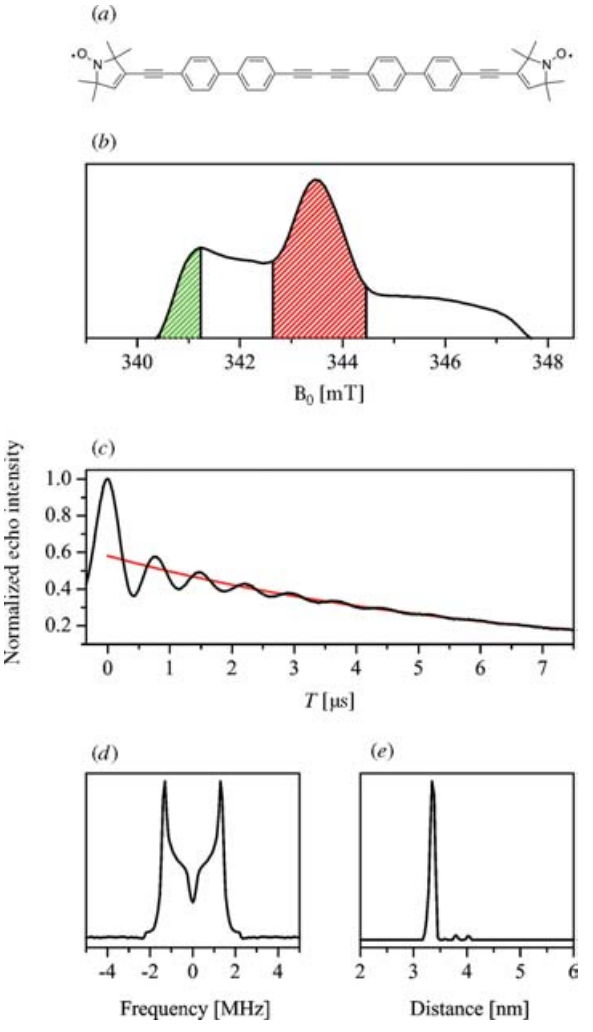

Fig. 4. PELDOR on a bisnitroxide model system. (*a*) Structure of a model biradical with an end-to-end distance of 34·7 Å and (*b*) its two-pulse Hahn-echo field swept spectrum. The portions of the spectrum excited by the detection and inversion pulses are depicted in green and red, respectively. (*c*) The four-pulse PELDOR time trace (black line) together with the fitted intermolecular background decay (red line). (*d*) Fourier transformation of the dipolar modulation time trace with peaks at 1·3 and 2·3 MHz, corresponding to $\theta_{\perp}$ and $\theta_{\parallel}$, respectively. From these frequencies a distance of 35·2 Å and an exchange coupling constant J of $-0{\cdot}1$ MHz is calculated as outlined in Section 2.1 (*e*) Tikhonov regularization of the same time trace, reveals a mean distance of $r = 33{\cdot}4$ Å and a width at half height of $\pm 0{\cdot}5$ Å. The Tikhonov regularization does not take the exchange coupling into account.

The intermolecular dipolar interaction between the different spin clusters in the sample with an absolute spin concentration c introduces an additional exponential attenuation of the signal:

$$V(T)_{\text{total}} = V(T) \cdot \exp\left(-\frac{\lambda \cdot \gamma_{\text{A}} \cdot \gamma_{\text{B}} \cdot c \cdot T}{\hbar}\right), \tag{12}$$

where $V(T)$ is given by Eq. (10). The exponential decay due to intermolecular interactions has to be removed from $V(T)_{\text{total}}$, before the distance R and the number of coupled spins N can be

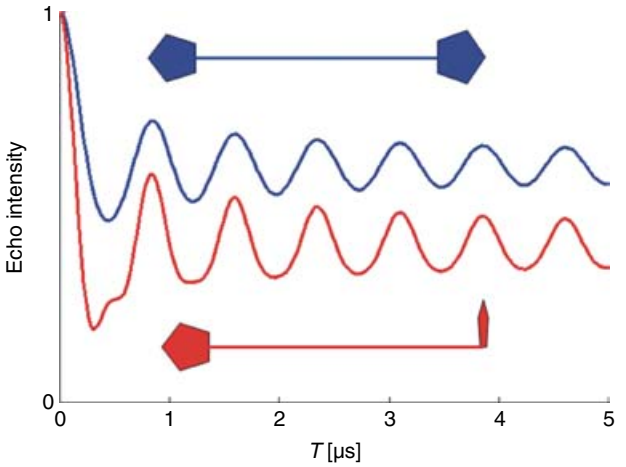

Fig. 5. Influence of different spin label orientations on the PELDOR time trace.

extracted. To reduce the intermolecular contribution, spin concentrations of $c < 200$ µM should be used. Additionally, aggregation of molecules has to be avoided. To determine the intermolecular exponential decay, $V(T)$ has to be fitted at long times T, where only this part contributes to the signal decay (see Fig. 4*c*). All these constraints set a lower limit to the pulse separation time τ, which might be difficult to fulfill in biological samples with low signal-to-noise ratio and fast intrinsic relaxation time T_2 of the nitroxide radicals.

To solve Eq. (11) for N, it is important to record the signal V_0 at $T = 0$. With the three-pulse sequence this is for most experimental setups impossible, because an overlap of the first detection pulse with the inversion pulse introduces experimental artifacts. A four-pulse sequence (see Fig. 2) overcomes this problem by refocusing the primary two-pulse Hahn-echo with an additional π-pulse of frequency ν_A. The primary Hahn-echo at time 2τ corresponds now to $T = 0$ and dead-time free signals can be recorded by stepping the inversion pulse between the two π-pulses (Martin *et al.* 1998). The usage of phase cycling eliminates experimental amplitude offsets to the echo function $V(T)$ and the Pake pattern is obtained free of experimental distortions allowing to accurately measure the distance R and the exchange coupling J (Pannier *et al.* 2000).

2.3.1.2 Orientation selection

For rigid biradicals, where the relative orientations between the two radicals and to the connecting vector R are fixed, the extraction of distances and numbers of coupled spins is more demanding. Firstly, the orientation selection $h(\theta)$ of the excitation of spin A will lead to a non-random detection of dipolar angles θ and consequently to the observation of a distorted and incomplete Pake pattern. In this case the integration of the signal is more complex (Larsen & Sigel, 1993):

$$V(T) = V_0\left(1 - \int_0^{\pi/2}\left[\lambda + \lambda\cos\left(\frac{D_c}{R^3}(1 - 3\cos^2\theta)\,T\right)\right]\cdot h(\theta)\sin\theta\,d\theta\right). \tag{13}$$

Secondly, also the modulation depth parameter λ depends now on the angle θ. This orientation dependence of λ may lead to different signal intensities for large T. Thus, the observed dipolar frequency spectrum cannot be converted directly to a distance R, if the relative orientations are unknown. This is shown in Fig. 5, displaying simulated PELDOR time traces for two theoretical

biradicals with rigid structures. In the first case, the molecular z axes of the two nitroxides are chosen parallel to each other and both are perpendicular to R. In the second case, the two molecular z axes are perpendicular to each other, one being parallel and the other perpendicular to R. In this example, different offsets for large values of T as well as different frequency components in the oscillations can be observed. To unravel orientational and distance information in such cases, the excitation and pump frequencies can be varied to excite and pump different subensembles of the disordered biradical. This can be experimentally better achieved at higher microwave frequencies and high magnetic fields (see Section 2.7).

2.3.1.3 Data analysis

The maximum distance that can be extracted depends on the length of the recorded time trace due to Fourier arguments. It is limited by the intrinsic transversal relaxation properties of the A spin. For nitroxide radicals at 60 K it is typically in the order of a few microseconds, depending on the solvent. A maximum T of 3 μs corresponds to an oscillation frequency $\omega_{\mathrm{dip}}/2\pi$ of 300 kHz and a distance R of 5·5 nm. Longer distances are accessible with extended time windows or high signal-to-noise ratios. Extended time windows may be achieved with improved signal-to-noise ratio via a variable τ_2 experiment (Jeschke *et al.* 2004a).

In cases where either more than two paramagnetic molecules with different distances are coupled or where large conformational distributions of R occur, more elaborate time domain fitting methods have to be used to accurately determine distance distributions and relative intensities. Tikhonov regularization can be performed to gain information of the distance distribution $P(R)$ directly from the time domain trace (see Fig. 4*e*). This is a very efficient numerical algorithm to gather consistent and stable results in 'ill-defined' problems, where small variations in the experimental data may lead to rather different solutions of the desired function. For orientationally uncorrelated radicals, the oscillatory part of the signal $V(T)$ can be written as (Jeschke *et al.* 2004b; Chiang *et al.* 2005a):

$$V(T) = \int_{R_{\min}}^{R_{\max}} \kappa(R, T) \cdot P(R)\, \mathrm{d}R, \tag{14}$$

$$\kappa(R, T) = \int_0^1 \cos\left[(1-3x^2)\frac{D_{\mathrm{dip}}}{R^3}T\right] \mathrm{d}x, \tag{15}$$

with $x = \cos\theta$. Assuming a smooth distribution $P(R)$, this method can be used to simulate time traces and to extract the distance distribution function $P(R)$ far better than by direct Fourier transform and visual inspection of the resulting Pake pattern. The additional constraint of $R > 0$ can be incorporated via a consecutive maximum entropy regularization (Chiang *et al.* 2005b).

Orientational selection and correlation hampers the simulation of the time domain data as the selection of A and B spins depends not only on the experimental pulse lengths, field strengths, and frequencies, but also on the relative orientations of the two nitroxides with respect to each other and with respect to the R vector. In principle, Tikhonov regularization may still be applied, but the integral kernel function $\kappa(R, T)$ is complicated to formulate. If the simple integral kernel function presented above is used in such cases to extract $P(R)$, artificial peaks may occur which compensate the encoded orientational correlations. Therefore, like for all 'ill-defined' problems, careful processing of the experimental data is mandatory to avoid artifacts and over-interpretation. This is especially valid for time traces with a low signal-to-noise ratio,

without any visible dipolar oscillations, with modulations due to hyperfine couplings, with a short T time window or with fast intermolecular relaxation. Data should then be treated with care and rather conservatively. This description for the analysis of the data holds for all time domain dipolar methods described in this review. Computer programs for distance extractions from PELDOR time traces are available on the websites of G. Jeschke and J. H. Freed.

2.3.2 The '2 + 1' pulse sequence

The two-frequency PELDOR method is, from an experimental point of view, more demanding than the earlier introduced single-frequency version called '2 + 1' (Kurshev *et al.* 1988). Firstly, two different microwave sources have to be used and secondly the quality factor Q of the microwave resonant circuit has to be lowered to achieve the necessary bandwidth to support both frequencies. Nevertheless, PELDOR has been more successfully employed to determine distances between spin pairs. One of the reasons is that the additional degree of freedom with two independent microwave frequencies allows to adjust the experiment better for optimum spectral pump and detection positions. Additionally, the '2 + 1' method does not work well for strong pumping efficiencies due to strong interference of pump and probe spins. The major disadvantage of the single frequency '2 + 1' method is that the desired dipolar oscillation may be obscured by hyperfine modulation artifacts. These artifacts are strongly reduced in the two-frequency PELDOR experiment, where the two microwave sources are not phase coherent to each other (Raitsimring *et al.* 1995).

Even in the two-frequency PELDOR experiment, the dipolar modulation may be blotted by hyperfine artifacts, especially if the dipolar modulation is weak. However, hyperfine frequencies can be distinguished from electron–electron dipolar couplings by performing PELDOR experiments at different magnetic field strengths (Weber *et al.* 2002). The hyperfine frequencies shift upon changing the external magnetic field, whereas the dipolar interaction frequencies remain the same. Hyperfine modulations are also suppressed in the four-pulse sequence by either adjusting τ to minima for specific hyperfine frequencies (blind spots) or by averaging PELDOR time traces recorded with different τ_1 values so that the hyperfine modulations diminish due to phase interference (Jeschke *et al.* 2004b).

2.3.3 Solid-echo experiment

Another way to observe the dipolar coupling is the solid echo-pulse sequence ($(\pi/2)_x - \tau - (\pi/2)_y - \tau$-echo) known from NMR spectroscopy (Mehring & Weberruß, 2001). To achieve a sufficient refocusing in EPR, with broad lines and off-resonant spins, two additional π pulses have been symmetrically inserted into the two evolution time segments (see Fig. 2) in the SIFTER (single-frequency techniques for refocusing) pulse sequence (Jeschke *et al.* 2000). For $\tau_1 = \tau_2$, the dipolar coupling is fully refocused and for $\tau_1 \neq \tau_2$, the intensity of the echo signal $V(\tau_2 - \tau_1)$ reflects the dipolar coupling. Ideally, this experiment requires that the whole EPR line is excited. Therefore, it suffers, as any multi-pulse sequence in EPR, from non-ideal excitations, which partially allow unwanted coherence pathways to contribute to the observed signal. A spin-alignment sequence, as the Jeener–Broekaert echo sequence in NMR (Mehring & Weberruß, 2001), can be used to minimize some of these unwanted signal contributions, but it strongly reduces the echo intensity and is less efficient than the double quantum filter explained below.

2.4 Double-quantum coherence EPR

An elegant way to solely detect the dipolar electron–electron coupling in a time-domain experiment is by introducing a double-quantum coherence filter into the pulse sequence, similar to multiple-quantum NMR experiments (Ernst *et al.* 1990). In contrast to liquid-state NMR, this experiment is extremely challenging in EPR, because of the large spectral width of the nitroxide spin labels, which have to be fully excited for an optimum performance. Such an experiment has, nevertheless, been successfully carried out by the group of Freed with a home-built pulsed K-band (17 GHz) EPR spectrometer, which exhibits very strong B_1 fields and a short dead time. They used an optimized six-pulse sequence (see Fig. 2) together with appropriate phase cycling to suppress all unwanted coherence pathways (Borbat & Freed, 1999). The sequence consists of three echo sandwiches: in the first and third segment single quantum coherence evolves under the dipolar coupling Hamiltonian. The second echo sandwich serves together with the appropriate phase cycle as a double-quantum filter in the coherence pathway of the observable signal $V(t_2 - t_1)$ and suppresses all contributions not related to dipolar coupled spin pairs. The intermolecular interaction to other electron spins and spectral diffusion can be removed from the time trace by inspection of the signal decay for large time offsets from the refocusing position ($t_1 = t_2$), similar to the PELDOR experiment. The interference with electron-nuclear modulation effects is strongly reduced and shifted to frequencies larger than the dipolar frequencies at higher magnetic field values. The chosen K-band frequency might already be the optimum for nitroxide radicals, since the full excitation of the whole spin system becomes increasingly difficult at higher fields due to the larger spectral widths.

Different from the PELDOR experiment, a full excitation of both radicals has to be achieved for optimal performance, which leads in principle to a larger signal intensity and a bigger modulation depth than PELDOR. Yet, the sample size has to be restricted to the center part of the resonator to perform the experiment with maximum and homogeneous microwave field strength. Additionally, the maximum achievable B_1 field strength is still not large enough to obtain optimized coherence transfer efficiencies. Therefore, the signal quality of double-quantum coherence (DQC) experiments is at the moment just similar to PELDOR experiments, even under best experimental conditions (Freed, 2000) and has been applied convincingly only by the Freed group.

The direct generation of double-quantum coherences is not efficient in the case of weaker microwave pulses as obtainable by commercial instruments. In such cases it is possible to excite double-quantum coherences by forbidden transitions (Saxena & Freed, 1996), but hyperfine modulation artifacts will be very difficult to suppress. They are diminished to a certain extent by variation of the observation window (Bonora *et al.* 2004), but this leads to additional loss in the signal-to-noise ratio.

In contrast to the PELDOR experiment, DQC-EPR does not suffer from orientational selection or orientation-dependent inversion efficiency. If angular correlations between the two coupled spins exist, a 2D version of the experiment (Freed, 2000) would allow to disentangle orientation from distance information. Furthermore, DQC-EPR might also be applicable to distances shorter than 15 Å (Freed, 2000).

2.5 Photo-excited radical pairs

A special situation exists for radical pairs created by fast charge separation after photo-excitation out of a singlet ground state. In this case the radical pair is generated with a high non-Boltzmann

population. Only $|\alpha\beta\rangle$ and $|\beta\alpha\rangle$ states are created as longitudinal two-spin order with an initial zero-quantum coherence between these two states (Salikhov *et al.* 1990; Zwanenburg & Hore, 1993). Under these special preparation conditions, the dipolar coupling between the two spins can be detected with a variety of rather unique experiments described in the following sections.

2.5.1 Zero-quantum coherence beat experiment

The zero-quantum coherence, created by the fast radical pair generation, can be monitored directly by fast time-resolved EPR. The oscillation frequency is governed by the balance between the Larmor frequency difference between the two spins and their dipolar and exchange coupling. Therefore, this quantum-beat experiment allows to obtain the dipolar coupling strength and the distance between the radicals within the radical pair (Salikhov *et al.* 1990; Bittl & Kothe, 1991).

2.5.2 Transient EPR

Even after the attenuation of these short-lived, coherent zero-quantum oscillations (typically 100–1000 ns), the spin system is far from Boltzmann equilibrium. This leads to strong superimposed absorptive and emissive transitions to the $|\alpha\alpha\rangle$ and $|\beta\beta\rangle$ states, respectively, which can be measured by transient time-resolved EPR spectroscopy. The spectra of these two signals would cancel each other exactly if they were not shifted with respect to each other by the dipolar and exchange coupling frequencies. The highly structured spectrum with emissive and absorptive components is very sensitive to the dipolar coupling strength and the relative orientation of the R vector with respect to the molecular axes systems of the two paramagnetic centers. The relative orientation between the two radicals can be obtained at high magnetic fields, where the spectrum is dominated by the anisotropic g tensor (Stehlik & Möbius, 1997).

2.5.3 Out-of-phase echo

In principle, a simple two-pulse Hahn-echo decay, recorded as a function of τ, is already modulated by the dipolar coupling if both spins are efficiently excited by the microwave pulses. Usually this can hardly be observed in a direct manner, because other effects such as transversal relaxation and hyperfine modulation dominate the signal $V(\tau)$. The situation differs for photo-excited radical pairs. The spin alignment of the two spins after photo-excitation leads to a peculiar echo signal that can only be observed for a non-zero dipolar coupling and with a 90° phase shift with respect to the usual Hahn-echo signal (Timmel *et al.* 1998). This unusual echo signal is modulated by the dipolar coupling, which can be directly observed as a function of the pulse separation time τ (Dzuba *et al.* 1995).

2.6 Relaxation methods

All pulsed-EPR methods described so far rely on an inversion pulse efficiently flipping the B spin and a longitudinal relaxation time T_1 of the B spins that is larger than the observation time T. For metal centers, both conditions can, in most cases, not satisfactorily be fulfilled. Nevertheless, if the B spin relaxes much faster than the A spin, then the B spin flips during the observation

time window, even without inversion pulse, due to its short intrinsic longitudinal relaxation time T_1^B. Because of the statistical nature of these spin flips, the effect of the dipolar coupling will not bear any coherent oscillations, but only add an additional monotonous attenuation to the signal decay of spin A. If the longitudinal relaxation process of spin B is not correlated with the intrinsic relaxation mechanism of the A spin, the attenuation of the A spin signal will be a product of this intrinsic relaxation and the dipolar relaxation due to the interaction with spin B. If the intrinsic relaxation properties of spin A are known independently, the dipolar relaxation contribution can be separated. Depending on the value of the longitudinal relaxation time T_1^B the dipolar relaxation will effect either the transversal or longitudinal relaxation properties of spin A.

2.6.1 Transverse dipolar relaxation

If the longitudinal relaxation rate $1/T_1^B$ of spin B is in the order of the dipolar splitting frequency ω_{dip}, the dipolar relaxation will mostly effect the transversal relaxation of spin A.

The transversal dipolar relaxation enhancement can be determined by monitoring the decay of a two-pulse Hahn-echo as a function of 2τ. The decay of the echo amplitude $V(2\tau)$ is then $T_{2,dip}^A$ as described by Zhidomirov & Salikhov (1969) and Salikhov *et al.* (1976, 1981):

$$V(2\tau) = C^{-2}\left[\frac{K}{2}\left((K+C)e^{-(K-C)2\tau} + (K-C)e^{-(K+C)2\tau}\right) - \tfrac{1}{4}\omega_{dip}^2 e^{-K2\tau}\right], \tag{16}$$

with $C = \sqrt{K^2 - \tfrac{1}{4}\omega_{dip}^2}$ and $K = 1/T_1^B$.

For the two cases $1/T_1^B \ll \omega_{dip}$ and $1/T_1^B \gg \omega_{dip}$ the following approximate solutions can be derived:

$$\text{for } \frac{1}{T_1^B} \ll \omega_{dip} \Rightarrow \frac{1}{T_{2,dip}^A} = \frac{1}{T_1^B} \tag{17}$$

and

$$\text{for } \frac{1}{T_1^B} \gg \omega_{dip} \Rightarrow \frac{1}{T_{2,dip}^A} = \frac{\omega_{dip}^2 \cdot T_1^B}{2} \tag{18}$$

Equations (16)–(18) show that the dipolar relaxation enhancement is maximal for $1/T_1^B = \omega_{dip}$. Because the relaxation time T_1^B depends on the temperature, a temperature-dependent measurement of the transversal relaxation of spin A can be used to optimize the dipolar relaxation effect and to extract the dipolar coupling strength from the relaxation enhancement.

2.6.2 Longitudinal dipolar relaxation

If the longitudinal relaxation rate $1/T_1^B$ of spin B is in the order of the larmor frequency ω_A of spin A, the dipolar relaxation will predominately effect the longitudinal relaxation of spin A. A pulse sequence commonly used to measure the longitudinal relaxation is the inversion recovery sequence (see Fig. 2). The intrinsic longitudinal relaxation properties of the A spin have to be known to extract the dipolar relaxation enhancement. This dipolar relaxation enhancement

on the longitudinal relaxation rate $1/T_1^{\mathrm{A}}$ is given by Kulikov & Likhtenstein (1977) and Rakowsky *et al.* (1995):

$$\left.\begin{aligned}\frac{1}{T_{1\mathrm{A}}^{\mathrm{dip}}} = {} & \frac{8}{3}\cdot\frac{T_{2\mathrm{B}}}{1+(\omega_{\mathrm{A}}-\omega_{\mathrm{B}})^2T_{2\mathrm{B}}^2}\cdot\left[\frac{\gamma_{\mathrm{A}}\mu_{\mathrm{B}}}{4R^3}(1-3\cos^2\theta)\right]^2 \\ & + \frac{3}{2}\cdot\frac{T_{2\mathrm{A}}}{1+(\omega_{\mathrm{A}}+\omega_{\mathrm{B}})^2T_{2\mathrm{B}}^2}\cdot\left[\frac{\gamma_{\mathrm{A}}\mu_{\mathrm{B}}}{R^3}(\sin^2\theta)\right]^2 \\ & + \frac{3T_{1\mathrm{B}}}{1+\omega_{\mathrm{A}}^2T_{1\mathrm{B}}^2}\left[\frac{\gamma_{\mathrm{A}}\mu_{\mathrm{B}}}{R^3}\sin\theta\,\cos\theta\right]^2,\end{aligned}\right\} \tag{19}$$

where ω_{A} and ω_{B} are the resonance frequencies of spins A and B, respectively.

The disadvantage of relaxation methods is that the dipolar effect only leads to an additional exponential decay of the signal and not to a coherent oscillation, because of the statistic nature of the spin-flip processes. Separation of this contribution from intrinsic relaxation mechanisms is not trivial. Furthermore, distance and orientation information are both encoded in this monotonous decaying time trace. Therefore, orientation-selective and temperature-dependent measurements are important to disentangle the information and to obtain quantitative results (Hirsh *et al.* 1992).

2.6.3 RIDME

A stimulated echo sequence (see Fig. 2) can also be used to measure the dipolar coupling between the spins. In contrast to the relaxation methods described above, this method, called relaxation induced dipolar modulation enhancement (RIDME) (Kulik *et al.* 2001), yields a time trace in which the dipolar coupling manifests itself as an oscillation, similar to the PELDOR experiment. The first two $\pi/2$ pulses of a stimulated echo sequence create a periodic modulation of the M_z magnetization as a function of the Larmor frequency with a periodicity given by $1/\tau$. The third $\pi/2$ pulse applied after a time T converts this grating into transversal magnetization which leads to an echo-like free induction signal, with a maximum at a time τ after this pulse. The amplitude of this signal is proportional to the amount of grating left at the time of the third pulse (Mims, 1972). The M_z modulation can be destroyed by longitudinal relaxation processes or by spectral diffusion. Larmor frequency jumps of the spin A induced by spin flips of the fast relaxing B spin belong to this second category (Salikhov *et al.* 1981). The attenuation of the stimulated echo intensity is strongest if a spin A jumps from a maximum of the grating to a minimum, corresponding to the condition $\omega_{\mathrm{dip}} = (2k+1)\pi/\tau$ with $k = 0, 1, 2, 3, \ldots, \infty$. Therefore, a measurement of the echo signal intensity $V(\tau)$ will exhibit a periodic oscillation with ω_{dip}, assuming that the pulse separation time T is chosen long enough to allow an efficient flipping of the spin B due to longitudinal relaxation. Unfortunately, hyperfine modulation and transversal relaxation will obscure the effect, as in a two-pulse echo sequence. Therefore, this experiment is best performed at high magnetic field values, where hyperfine modulations are strongly reduced (Kulik *et al.* 2002).

2.7 High-field EPR

At high magnetic field values, the microwave resonance frequency (Larmor frequency ω_{L}) is given by

$$\omega_{\mathrm{L}} = \beta_{\mathrm{e}}\cdot g_{\mathrm{eff}}(\theta,\varphi)\cdot B_0 \tag{20}$$

with

$$g_{\text{eff}}(\theta,\varphi) = \sqrt{\sin^2\theta\cdot\cos^2\varphi\cdot g_x^2 + \sin^2\theta\cdot\sin^2\varphi\cdot g_y^2 + \cos^2\theta\cdot g_z^2}\,, \tag{21}$$

where θ and φ are the polar angles of the magnetic field direction within the axis system of the molecular g tensor. This Zeeman interaction dominates at large values of the magnetic field and allows to resolve the principal g-matrix elements (g_x, g_y, g_z) of the paramagnetic center, because most other interactions, e.g. hyperfine or dipolar coupling constants, are not field-dependent (see Fig. 3). Deviations of the principal g values from the free electron g_e value (2·0023) arise from residual orbital momentum of the unpaired electron. They can be used as a simple fingerprint to identify the radical species or in comparison with quantum chemical calculations to investigate hydrogen bonds, ligand geometry, and the electrostatic surrounding of the paramagnetic center in a biological system.

If the g tensor is anisotropic, molecules with different orientations with respect to the external magnetic field will have different resonance field values. Thus, it is possible to experimentally select in disordered samples molecules with a specific orientation to B_0 by means of the microwave frequency or the external field value. This so-called orientation selection enables to measure the anisotropy of other interactions with respect to the g tensor axis system. The method is of particular interest for the measurement of anisotropic hyperfine interactions by electron nuclear double resonance (ENDOR) or of dipolar interactions by PELDOR or RIDME to obtain the relative orientations of the coupled nuclei or paramagnetic center within the g tensor axis system. With respect to PELDOR, this was shown on dipolarly coupled spin systems with fixed geometry, as described above (Bennati & Prisner, 2005; Denysenkov *et al.* 2006) and recently also for a more flexible system (Polyhach *et al.* 2007).

Unfortunately, the increased spectral resolution is also a disadvantage for pulsed-EPR experiments. The extended spectral width leads to a smaller number of detected spins A and inverted spins B in a PELDOR experiment, resulting in smaller signal intensity and a shallow modulation depth. Furthermore, not all spectrally possible combinations of excitation and detection frequencies can be chosen because of experimental restrictions with respect to the resonator bandwidth. Therefore, high sensitivity and stability of the spectrometer are crucial to perform high-field (HF) PELDOR experiments. Experiments relying on dipolar relaxation are not limited by this reduced pumping efficiency at higher fields and may thus gain more importance for the investigation of dipolarly coupled spin systems (Kulik *et al.* 2002).

The circumstances are different for half-integer high-spin systems, as for example Mn^{2+}. The central transition from $m_S = -\frac{1}{2}$ to $m_S = +\frac{1}{2}$ is actually narrower as compared to lower field, due to a reduced linewidth contribution from zero-field splitting. In such cases, an increased cw-HF-EPR sensitivity towards dipolar couplings arises (Käss *et al.* 1998) and higher pumping efficiencies are obtained. Additionally, the spectral overlap between signals from paramagnetic centers is reduced, e.g. between a nitroxide and a manganese(II) ion, enabling superior experimental conditions for a PELDOR experiment. As soon as the technical conditions of such HF-EPR spectrometers are further improved with respect to microwave field strength, stability and resonator bandwidth (Prisner, 1997), these experiments will become even more important for orientationally correlated radicals, as found for natural cofactors in proteins.

3. Model systems

In order to investigate the application range and limitations of an EPR pulse sequence capable of measuring longe-range electron–electron distances, a large library of bisnitroxide model systems

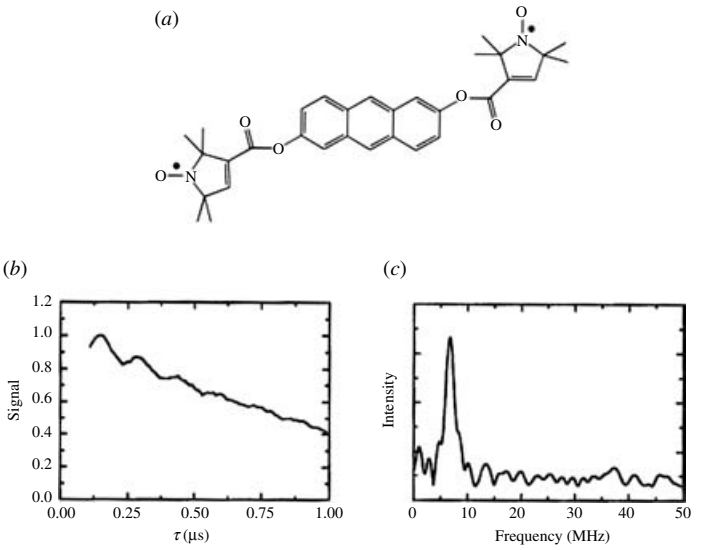

Fig. 6. First observation of dipolar modulations in PELDOR. (*a*) Structure of the model system 2,6-bis[(((2,2,5,5-tetramethyl-1-oxypyrrolin-3-yl)carbonyl)oxy)]-anthracene ($r = 19{\cdot}6$ Å) and (*b*) its 3-Pulse ELDOR time trace (77 K). (*c*) Modulus Fourier transformation of the time trace with a peak at 6·8 MHz, corresponding to a distance of 19·7 Å (Larsen & Singel, 1993).

has been synthesized and especially used for PELDOR. Singel and Larsen were the first to demonstrate the applicability of three-pulse ELDOR for measuring fixed distances (Larsen & Singel, 1993) using an anthracene molecule connecting two nitroxides (see Fig. 6). The four-pulse ELDOR sequence was tested first on a series of rigid rod-like bisnitroxides covering a distance range from 14 to 28 Å (Martin *et al.* 1998; Pannier *et al.* 2000). This collection of model systems has been extended to spin–spin distances of 51 Å (Godt *et al.* 2000) and later to 75 Å (Jeschke *et al.* 2004a) utilizing a combination of aryl and ethynyl groups as spacers (see Fig. 7). Similar model systems have also been used for SIFTER (Jeschke *et al.* 2000) and DQC-EPR (Borbat & Freed, 2000) distance measurements. In a recent paper, the dynamics of these molecular nano-rods were studied by PELDOR and MD simulations (Godt *et al.* 2006), proving that PELDOR can yield distance distributions, which translate into dynamics at room temperature. The applicability to more flexible systems remains to be investigated, but first examples of two nitroxides linked via alkyl chains of different length are published (Pfannebecker *et al.* 1996; Jeschke *et al.* 2002; Jeschke & Schlick, 2006). Bisnitroxides with bridges with or without conjugated bonds have been synthesized to demonstrate the separation of exchange coupling J from ω_{dip} (Weber *et al.* 2002).

A rigid imidazoline bridged biradical with an end-to-end distance of 20 Å and a bisnitroxide with 2,6-bisthiophene-cyclohexanone as a more flexible linker have been employed for studying RIDME (Kulik *et al.* 2001) and DQC-EPR with small B_1 field strength and suppression of hyperfine artifacts (Bonora *et al.* 2004), respectively. In another work, two nitroxides were coupled to a Cu^{2+}-complex, but the compound was not isolated (Narr *et al.* 2002). For PELDOR distance measurements on nonbiological materials, we refer the reader to Jeschke *et al.* (2002). Thus, not only rigid bisnitroxide model systems spanning distances from 14 to 75 Å, but also such with different degrees of flexibility are available. Regarding multiple spin systems, Godt *et al.* described the synthesis of one triradical (Godt *et al.* 2000) and Bode *et al.* published recently the

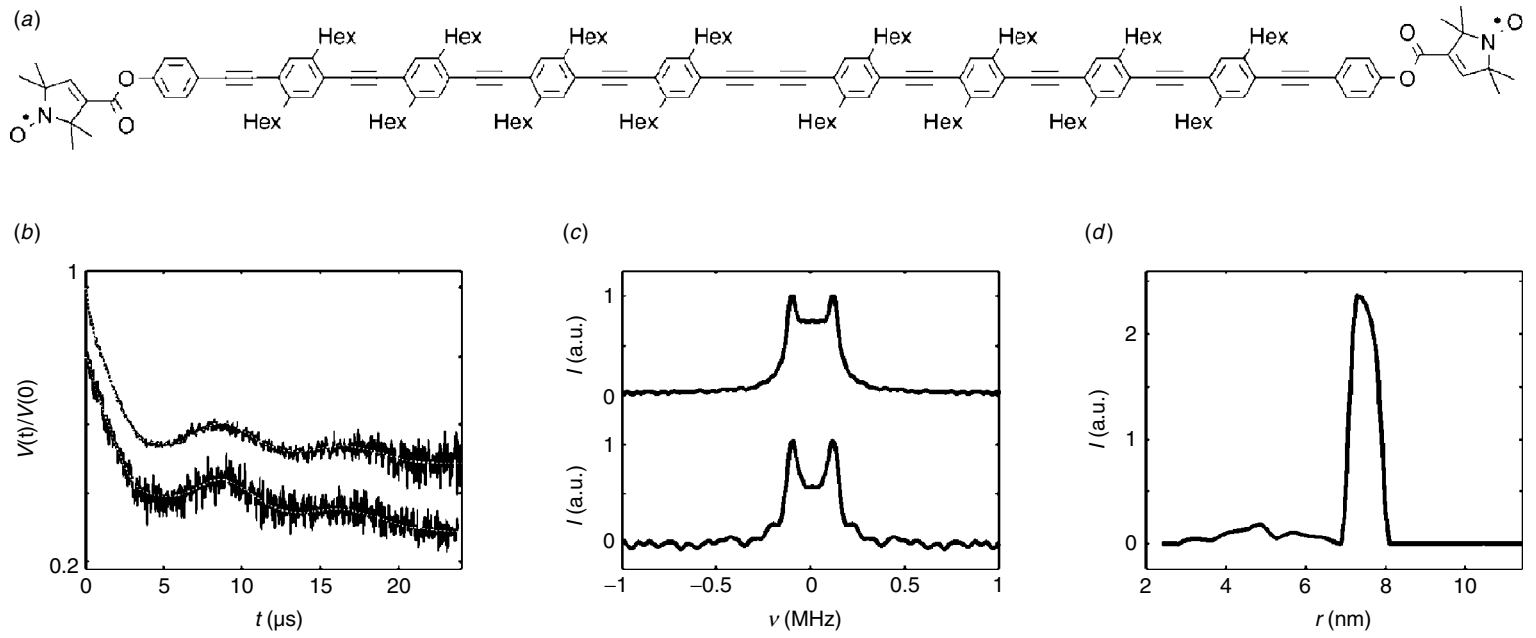

Fig. 7. A shape-persistent biradical with the longest inter-spin distance measured by PELDOR. (*a*) Structure of the biradical. (*b*) Time trace of the biradical in perdeuterated glassy *o*-terphenyl using variable time four-pulse ELDOR (top) and four-pulse ELDOR (bottom). The dashed lines are fits. (*c*) Fourier transformation, and (*d*) Tikhonov regularization of the time trace. Tikhonov regularization yielded a mean distance of 74·9 Å and a width at half-height of about 8 Å (Jeschke *et al.* 2004a).

a series of bi-, tri- and tetra radicals with different distances and geometries and showed on these that spin counting is possible for pure multi-spin systems but becomes complicated for mixtures (Bode *et al.* 2007). Also PELDOR measurements on ^{15}N-, ^{2}H-isotope labeled biradicals as test systems for distance assignments in multi-spin systems are described (Jeschke *et al.* 2006).

Concluding this chapter, it should be mentioned that all model systems have been examined in organic solvents, e.g. toluene or perdeuterated *ortho*-terphenyl, which leads to slow transversal relaxation times, enabling long observation time windows and thus the observation of large distances. To ensure that biomolecules adopt their biologically relevant structure, aqueous buffer solutions and maybe even membranes are to be favored over organic solvents. However, freezing an aqueous buffer solution does not lead to a random distribution of biomolecules, but rather to clustering and therefore to short intermolecular electron–electron distances. These close distances induce faster relaxation times and accordingly shorter observation time windows for PELDOR, '2 + 1' and DQC-EPR and increase the continuous wave EPR linewidths. In each case the accessible distance range is reduced. Cryoprotectants like glycerol or ethylene glycol can be added to avoid this limitation. Furthermore, deuterated buffers can be used to minimize transversal relaxation enhancement due to H_2O–nitroxide interactions.

4. Biological applications

EPR-based nanometer distance measurements are mainly applied to biological systems to study the arrangement of cofactors and subunits, the formation of secondary structure elements, or the interactions between biomolecules. In order to use EPR spectroscopic methods, the biomolecule has to contain either stable or transient paramagnetic centers, which can be metal ions or clusters, amino acid radicals, or organic cofactor radicals. If the biomolecule is diamagnetic, it can be spin-labeled with nitroxides or a diamagnetic metal may be substituted for a paramagnetic one.

In this section, we first give an overview of spin labeling and distance measurements in peptides and proteins, followed by studies related to arrangements of cofactors in proteins. Afterwards, we summarize spin labeling methods and distance measurements on RNA/DNA. Distance measurements involving metal centers or more than two spin centers are discussed separately at the end of this section.

4.1 Spin-labeled peptides and proteins

4.1.1 Spin labeling of peptides and proteins

Combining EPR spectroscopy with site-directed spin labeling was one of the major breakthroughs in biomolecular EPR spectroscopy (Berliner *et al.* 1982; Altenbach *et al.* 1990) and is reviewed in several monographs and articles (Berliner & Reuben, 1989; Likhtenshtein, 1993; Berliner, 1998; Hubbell *et al.* 1998; Berliner *et al.* 2000). The most commonly used spin label for site-directed labeling of proteins is a methanethiosulfonate-functionalized nitroxide called MTSSL, which reacts selectively with the thiol group of cysteines, forming a disulfide bridge. The label site can be selected and varied by site-directed mutagenesis, provided the structure and function of the protein are not disturbed. A slight drawback of the MTSSL label is the labile disulfide bridge connecting the nitroxide to the protein, because this bond might be cleaved under reducing conditions at room temperature. However, kept at 77 K, MTSSL-labeled proteins are stable over long periods of time. More stable linkers are formed by iodoacetamide- or maleimide-functionalized labels (Likhtenshtein, 1993), but the maleimide labels are less selective.

Peptides, accessible via solid-state peptide synthesis, can also be labeled with the rigid synthetic amino acid 2,2,6,6-tetramethylpiperidine-1-oxyl-4-amino-4-carboxylic acid (TOAC), which mimics the microbial amino acid α-aminoisobutyric acid (Aib) (Rassat & Rey, 1967; Marchetto *et al.* 1993).

4.1.2 Distance measurements on spin-labeled peptides

To gain insight into secondary structure elements of peptides, exploitation of the isotropic exchange coupling constant J between two spin labels was attempted (McNulty & Millhauser, 2000). The advantage of using the exchange coupling J as a measure for the distance R would be that it leads to a line splitting for liquid samples and biosystems with fast rotational correlation times. Indeed, continuous wave EPR spectra of a series of small peptides containing two TOAC labels, incorporated at various sequence positions, revealed different extents of exchange coupling in liquid solution at room temperature (Hanson *et al.* 1996). However, the translation of J into a distance is difficult since exchange coupling can be mediated not only through space but also through bond and thus depends on distances, bond orders, angles, and mechanisms (Kahn, 1993).

In contrast, all of the following experiments are based on the dipolar coupling ω_{dip}, which is only mediated through space and shows an R^{-3} dependence [see Section 2.1 and Eq. (5)]. This approach is usually limited to frozen samples or orienting media since ω_{dip} is averaged out in the liquid state. On the other hand, it permits to gather distances parameter free and orientation selective measurements might resolve the orientation of both spin centers with respect to each other. Yet, frozen samples give rise to the question whether the observed structure is still relevant under biological conditions. This restriction can be circumvented if the rotational correlation time of a molecule is larger than $\sim 1/\omega_{\mathrm{dip}}$ or by applying relaxation-based distance measurements (see Sections 2.6 and 4.4.3). In these cases, distance measurements can also be performed in the liquid state at physiological temperatures.

Rabenstein and Shin were the first to show in a systematic study that the dipolar coupling ω_{dip} can be extracted by Fourier deconvolution from continuous wave EPR spectra of frozen aqueous samples (Rabenstein & Shin, 1995). Their peptide ruler spans distances from 8 to 25 Å. The same range is accessible by means of simulating frozen solution EPR spectra (Hustedt & Beth, 2000). Smaller distances in the range from 4 to 15 Å can be attained via the relative intensity of the half-field transition (Anderson *et al.* 1999).

The first example for the application of PELDOR in the field of spin-labeled peptides was given by Milov *et al.* (1999) on two-fold TOAC-substituted trichogin. Their experiment yielded a distance of 19·7 Å and a narrow distance distribution of ± 1 Å, indicating a 2_7-configuration of the helix in a frozen chloroform/dimethylsulfoxide matrix (see also Section 4.5.1). A systematic PELDOR study on five end-labeled bis-peptides of different lengths in frozen aqueous buffer solution was published in 2006 (Pornsuwan *et al.* 2006). The measured distances show a linear increase from 23·8 to 34·6 Å and a broadening of the distance distributions with increasing number of peptide building blocks between the spin labels. This in combination with the good agreement with the mean distances of MD simulations proves the rigid rod-like structure of the bis-peptides. The observation that the experimental distribution width is smaller than the one from the MD calculations is attributed by the authors to a systematic overestimation of the bis-peptide flexibility by the MD. Another explanation might be that only a fraction of conformations populated at room temperature are trapped in the frozen state.

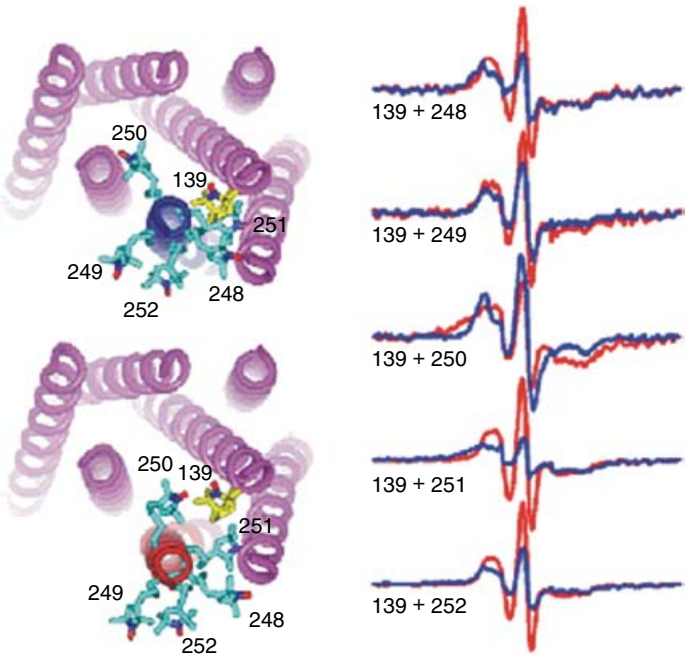

Fig. 8. Continuous wave EPR: Distance measurements between pairs of MTSSL labels attached to rhodopsin. For each pair, one label was attached to site 139, whereas the second label was varied through sites 248–252 in helix VI. The EPR spectra were recorded at room temperature and are shown on the right. The red traces correspond to the dark and the blue traces to the light-activated state. The light-induced movement of helix VI leads for each pair to a distance change, which reflects itself in a line width and amplitude change. A relative line broadening and decrease in amplitude indicates a decrease in inter-spin distance. while a line narrowing and increase in amplitude points to an increase in inter-spin distance (Hubbell *et al.* 2000).

DQC-EPR was applied to bis-labeled model peptides as early as 1996 by Freed and colleagues (Saxena & Freed, 1996, 1997; Borbat & Freed, 1999) and later with smaller B_1-fields and suppression of hyperfine artifacts by Saxena *et al.* (Bonora *et al.* 2004).

4.1.3 Distance measurements on spin-labelled proteins

4.1.3.1 Continuous wave EPR

Continuous wave EPR-based distance measurements between spin labels were successfully applied to investigate structures and structural changes of proteins, protein–protein, and protein–oligonucleotide complexes and have been reviewed already (Hustedt & Beth, 1999; Hubbell *et al.* 2000; Borbat *et al.* 2001; Perozo, 2002; Steinhoff, 2004). Here we would like to explicitly mention the work on the light-activation of rhodopsin as illustrated in Fig. 8 (Farrens *et al.* 1996), the work on the KcsA channel (Perozo *et al.* 1999; Liu *et al.* 2001), on the MscL channel (Perozo *et al.* 2002), and the archaeal sensory rhodopsin II/transducer complex (Wegener *et al.* 2001; Klare *et al.* 2004). All of these studies allowed the observation of functionally induced structural changes. It should, however, be stated that the conclusions drawn were not solely based on distance measurements, but backed up by additional EPR data like accessibility, mobility, and polarity. The proposed structure of the sensory rhodopsin II/transducer complex was in the meantime confirmed by X-ray diffraction (Gordeliy *et al.* 2002).

Four different approaches to extract distances from continuous wave X-band EPR spectra were tested on the well-characterized human carbonic anhydrase II (Persson *et al.* 2001). It was found that at very short distances, $R \leqslant 8$ Å, the relative ratio between the intensities of the half-field signal and the $g=2$ signal may be used. This approach, as well as using the ratio of peak heights as an indication for dipolar line broadening (Kokorin *et al.* 1972; Sun *et al.* 1999) is hampered by the presence of singly labeled molecules due to incomplete spin labeling. Fourier deconvolution and lineshape simulations worked well within a distance range of 8–20 Å, but both methods require, in particular for longer distances, linewidth information of the singly labeled protein as already shown by Rabenstein and Steinhoff (Rabenstein & Shin, 1995; Steinhoff *et al.* 1997). PELDOR time traces on carbonic anhydrase II revealed in one case an oscillation corresponding to a distance of 18 Å (Persson *et al.* 2001). Larger distances could not be accessed due to the short observation time window of 800 ns.

Hubbell and colleagues showed on T4 lysozyme that inter-spin label distances can also be extracted from continuous wave EPR spectra of proteins in liquid solution at room temperature, provided the overall rotation of the protein is in the slow motion regime (Yang *et al.* 1996; Hubbell *et al.* 2000; Langen *et al.* 2000; Altenbach *et al.* 2001). The dipolarly broadened spectra were fitted by convoluting the spectrum of the singly labeled species with a distribution of Pake patterns. The agreement between the distances obtained at room temperature, at cryogenic temperatures, and in the crystal structure makes this approach very promising. Furthermore, the distance distributions from the experiments are in accordance with MD simulations. On the other hand, this method only works in the narrow distance range from ~8 to ~18 Å and the error of the method is large in the presence of singly labeled proteins.

4.1.3.2 '2 + 1'/PELDOR

A '2 + 1' investigation on spin-labeled tetrameric hemoglobin (Raitsimring *et al.* 1992) was reported in 1992. The data analysis was, however, complicated by strong aggregation and hyperfine artifacts. Later studies on spin-labeled proteins were mainly PELDOR based, due to an improved suppression of these artifacts (Raitsimring *et al.* 1995).

PELDOR and continuous wave EPR methods were utilized to distinguish between two computational models for the inhibitory region of the cardiac troponin ternary complex. Based on the PELDOR constraints, this region appeared to be α-helical (Brown *et al.* 2002) in agreement with X-ray data, but disproving both computational models. Later it could be shown by PELDOR that binding of Ca^{2+} induces structural changes (Fajer, 2005). In a proof-of-principle study distances were gathered from PELDOR and continuous wave EPR, and relaxation measurements on the KcsA channel, troponin C, and the troponin complex (Sale *et al.*, 2005). These distances were compared with the respective C_β–C_β distances and with inter-spin distances obtained from MD simulations, taking the spin labels explicitly into account. The deviation was found to be large using just C_β–C_β distances, especially for shorter distances, whereas the overall deviation was only 3 Å over a distance range from roughly 5 to 45 Å with respect to the MD simulations.

The arrangement of the two β-subunits of the F_0F_1-ATP synthase from *Escherchia coli* was studied by labeling each subunit with a single spin label and measuring the resulting distance in the dimer with PELDOR (Steigmiller *et al.* 2005). The same distance of 29 Å was found for five different mutants, suggesting that the two helical subunits are aligned in a parallel fashion. Nevertheless, it could not be differentiated between an in-register alignment, with the two helices 19 Å apart from each other, and an arrangement where the two helices contact each other but are

shifted by 27 Å with respect to the same amino acid. These conclusions were again substantiated by continuous wave EPR polarity and mobility studies.

Continuous wave EPR and PELDOR experiments on the cytoplasmic domain of the anion exchange protein (cdb3) indicated that the global arrangement of the central dimer in solution at neutral pH is identical to the one in the crystals grown at pH 4·8 (Zhou *et al.* 2005). PELDOR time traces with oscillations were collected for the doubly spin-labeled protein in phosphate buffer with 30% glycerol. The C- and N-termini were found to be unstructured as in the crystal structure.

In one case, a spin label was attached to a native cysteine in the bacterial reaction center of *Rhodobacter sphaeroides* and the distance to the reduced primary acceptor Q_A was measured (Borovykh *et al.* 2006). The PELDOR time trace shows long-lived oscillations corresponding to a distance of $30{\cdot}5 \pm 0{\cdot}5$ Å and a distance distribution of $2{\cdot}4 \pm 0{\cdot}2$ Å. MD simulations at room temperature and at low temperature both revealed a slightly smaller distance of $28{\cdot}0 \pm 0{\cdot}5$ Å. Nevertheless, this approach might allow examination of small electron-transfer-induced structural changes at cofactor sites.

PELDOR studies on membrane-bound proteins showed only barely visible dipolar oscillations or exponential decays (Jeschke *et al.* 2004c; Jeschke *et al.* 2005; Borbat *et al.* 2006; Xu *et al.* 2006). In such cases, conclusions are mainly qualitative and should be drawn carefully. A major problem of spin-labeled proteins in membranes may be sample heterogeneity, caused by partial reconstitution, as well as clustering of proteins and vesicles and a fast relaxation time T_2 of the nitroxides.

4.1.3.3 DQC-EPR

The first application of DQC-EPR to a protein was a proof-of-principle study on T4 lysozyme (Borbat *et al.* 2002). Eight doubly MTSSL-labeled cysteine mutants were investigated by DQC-EPR at X- and K-band frequencies. All time traces revealed dipolar modulations, corresponding to distances from 20 to 50 Å, which fit nicely to the crystal structure of the protein. Distance distributions were analyzed with respect to linker flexibility and conformations. DQC-EPR was also utilized to investigate channel formation of gramicidin A in dependence of the type of lipid membrane (Dzikovski *et al.* 2004).

An example for the power of DQC-EPR/PELDOR is the work on the chemotaxis receptor-kinase assembly of *Thermotoga maritime* (Park *et al.* 2006). The structures of the CheW subdomain 2 and of the CheA domain P5 were known from NMR and X-ray analysis, respectively. The structural arrangement of both in the CheA:CheW complex was predicted based on 40 different long-range constraints collected by DQC-EPR/PELDOR experiments and was validated by the crystal structure of the CheA(P4, P5):CheW complex in the presence of the nonhydrolyzable ATP analog ADPNP (see Fig. 9). The measured distances cover a range from 14 to 70 Å and fit very well to the structure. Deviations in a few cases are overcompensated by the large amount of distance constraints. Implications for the mechanism of signaling were discussed based on the complex structure as well as biochemical studies.

4.2 Cofactors in proteins

4.2.1 Distance measurements on augmenter of liver regeneration

PELDOR was used to obtain structural information about the human augmenter of liver regeneration (ALR), a homodimeric sulfhydryl oxidase catalyzing the formation of disulfide bonds

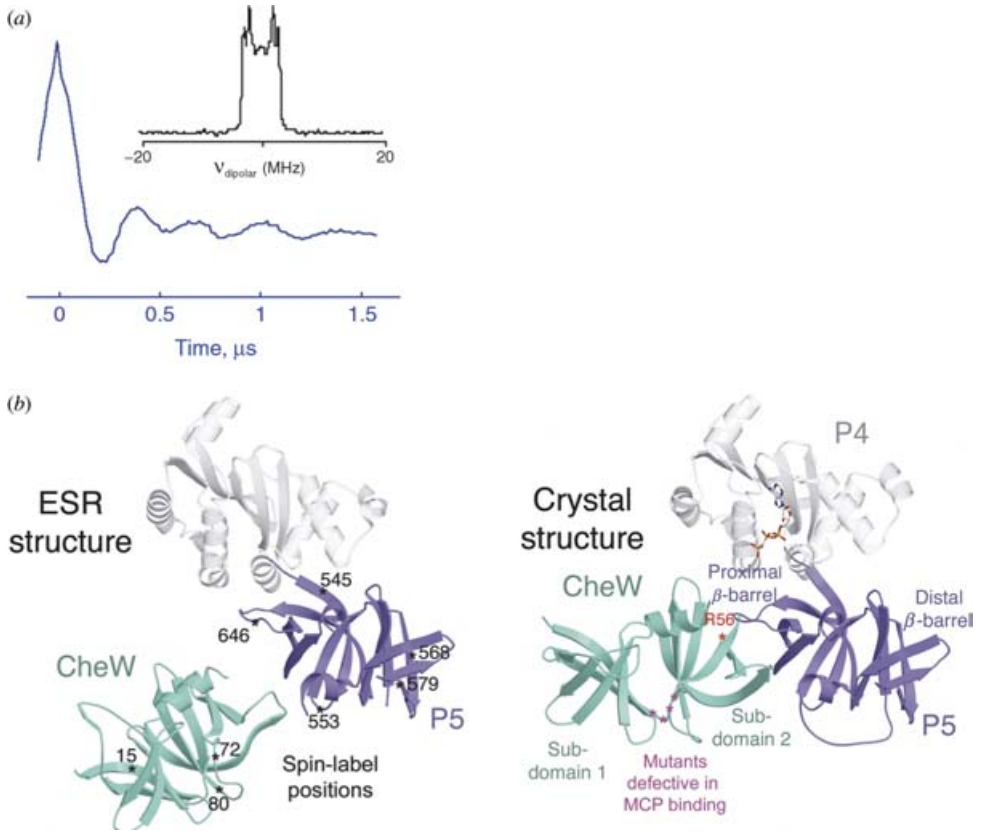

Fig. 9. DQC-EPR: Complex formation of the receptor-coupling protein CheW and the histidine kinase CheA. (*a*) DQC-EPR time trace for a CheA dimer labeled at site 318 and its Fourier transformation. (*b*) Arrangement of CheW subdomain-2 (NMR solution structure) and CheA domain P5 (crystal structure) in the CheA:CheW complex as predicted from DQC-EPR/PELDOR distance measurements. (*c*) Crystal structure (Park *et al.* 2006).

(Kay *et al.* 2006). Each of the two subunits contains a flavin, which can be reduced to a neutral flavin radical. The high yield of radical formation together with the fixed distance and orientation between both flavins allowed the observation of a deep and long-lived dipolar oscillation. Fourier transformation revealed both singularities of the Pake pattern permitting a parameter-free calculation of the distance to $26{\cdot}1 \pm 0{\cdot}8$ Å, which fits to the distance estimated from the crystal structure of rat ALR.

4.2.2 Distance measurements on ribonucleotide reductase

Ribonucleotide reductase (RNR) is a protein that catalyzes the conversion of nucleoside diphosphates to desoxynucleoside diphosphates. The mechanism of this conversion is not fully understood yet, but known to involve an electron transfer from a tyrosyl radical in the R2 subunit to the active site in the R1 subunit. It is proposed that the active protein is a 1:1 complex of the two homodimeric subunits R1 and R2 (Stubbe *et al.* 2003; Kolberg *et al.* 2004; Bennati *et al.* 2005a). The tyrosyl radical intermediates can be trapped with a yield of roughly one tyrosyl radical per R2 homodimer and can be detected EPR spectroscopically. A X-band PELDOR

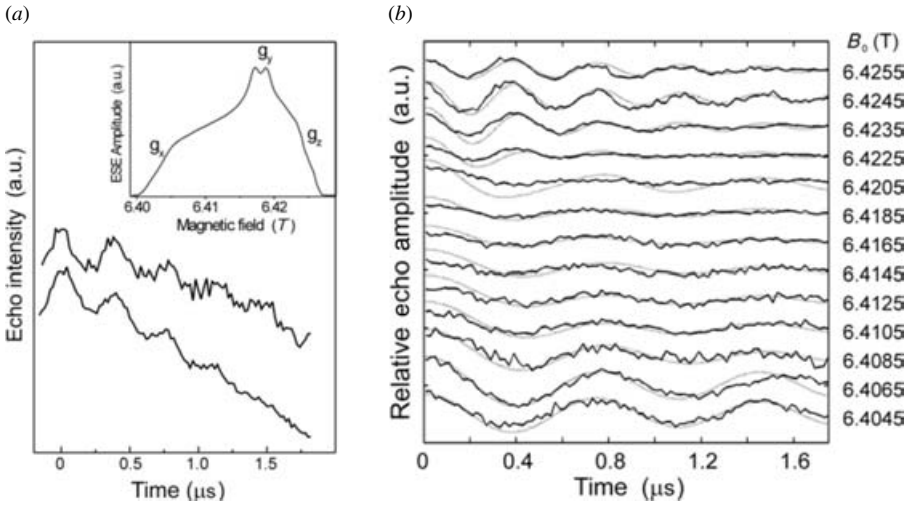

Fig. 10. High-field PELDOR: Distance and orientation between the two tyrosyl radicals in the R2 dimer. (*a*) Representative PELDOR time trace and the field-sweep EPR spectrum (inset). (*b*) PELDOR time traces acquired at different field positions after dividing by the intermolecular decay and the respective fits of the time traces (Denysenkov *et al.* 2006).

study on RNR from *E. coli* proved that in some cases two tyrosyl radicals are formed within one homodimeric R2 subunit *in vitro* and that the distance between them is 33·1 Å (Bennati *et al.* 2003). Taking spin density distributions into account, this distance is in accordance with the distance of 32·6 Å calculated from the crystal structure. The fact that dipolar oscillations were also found in PELDOR spectra of the R2 subunit of mouse RNR indicates that R2 is dimeric in some mammalian RNRs too (Biglino *et al.* 2006).

It was anticipated that the *g*-anisotropy of the tyrosyl radicals will lead to strong orientation selectivity at higher frequencies. Thus, a technical setup for PELDOR at 180 GHz was used (Denysenkov *et al.* 2005; Hertel *et al.* 2005) and subsequently applied to RNR (Denysenkov *et al.* 2006). Systematically varying the position of the pump and detection pulses over the field-swept spectrum revealed a well-resolved orientation selection visible in the PELDOR time traces (see Fig. 10). Simulating this orientation dependence of the dipolar coupling ω_{dip} allowed to obtain not only the distance, but also the mutual orientation of both the radicals. The orientation agrees well with *g* tensor studies at high field (Högbom *et al.* 2003) and both show the same small deviation of 10° with respect to the crystal structure of the nonradical state (Nordlund *et al.* 1990).

In the reaction of RNR with the inhibitor 2′-azido-2′-deoxyuridine-5′diphosphate (N_3UDP), an electron is transferred from the tyrosyl radical in the R2 subunit to the inhibitor in the R1 subunit, leading to the formation of a new nitrogen-centered radical, whose structure was recently solved (Fritscher *et al.* 2005). EPR measurements showed that both radicals, tyrosyl and inhibitor, are simultaneously present in the sample. PELDOR (X-band) as well as DQC-EPR (K-band) experiments led to fairly deep modulations for both methods from which Tikhonov regularizations extracted two distances (Bennati *et al.* 2005b): one of 33 Å, corresponding to the already known distance between the two tyrosyl radicals within the R2 subunit, and a new distance of 48·2 Å. Measurements at higher temperatures indicated that the larger distance belongs to the tyrosyl-inhibitor radical pair and not to the inhibitor–inhibitor pair. Using the

structural model based on R1:R2 docking studies, the authors found that the distance fits best to the distance between tyrosine and inhibitor located on different sites of the R1:R2 complex. This suggests that the electron-transfer proceeds over 35 Å, from the tyrosine to the inhibitor located both on the same site of the complex.

4.2.3 Distance measurements in photosystems

Photosynthetic proteins, like bacterial reaction centers (bRC), plant photosystem I (PS I), and photosystem II (PS II), are a special case with respect to EPR distance measurements. First of all, they are probably the most intensively studied protein complexes by EPR (Lubitz, 2004), and secondly the light-induced radical formation leads to spin polarization which demands unusual methods, as described in Section 2.5. These methods and their applications to photosynthetic proteins are well described in numerous reviews (Snyder & Thurnauer, 1993; Stehlik & Möbius, 1997; Lubitz & Feher, 1999; Dzuba & Hoff, 2000; Lakshmi & Brudvig, 2000; Bittl & Zech, 2001; Lubitz *et al.* 2002; Bittl & Weber, 2005). Bittl and Kawamori gave a good overview of EPR distance measurements in PS II, performed even before the crystal structures of PS II were known (Bittl & Kawamori, 2005). Here we summarize few examples involving organic cofactors. Measurements including metal centers in PS II are dealt with separately in Sections 4.4.2.2 and 4.4.3.2.

4.2.3.1 Bacterial reaction center

After the crystal structure was solved (Deisenhofer *et al.* 1986), the bacterial reaction center served as a benchmark system for distance determination by EPR methods. Transient spin-polarized EPR spectra were recorded as early as 1977 (Hoff *et al.* 1977) and interpreted in terms of dipolar distances later (Hore *et al.* 1987). The relative orientation of the chlorophyll dimer $P_{865}^{+\bullet}$ to $Q_A^{-\bullet}$ could be determined in addition to the distance of 28 Å by extending these experiments to higher microwave frequencies (Est *et al.* 1993; Prisner *et al.* 1995). Quantum-beat oscillations of the dipolar coupling shortly after the laser flash excitation were observed for this pair by transient EPR with high time resolution (Kothe *et al.* 1994). Also, out-of-phase echo envelope modulation was used to measure the distance in this radical pair (Dzuba *et al.* 1995) and to investigate postulated structural changes upon freezing procedures (Dzuba *et al.* 1997; Stehlik & Möbius, 1997; Borovykh *et al.* 2003). An out-of-phase FID detection of a selective hole-burning experiment was used to examine the dipolar interaction within the $^3P_{865}^{+\bullet}/Q_A^{-\bullet}$ radical pair, with the primary donor in the triplet state (Kulik *et al.* 2003).

4.2.3.2 Photosystem I

Research on the PS I of cyanobacteria or spinach led to the invention and application of many methods for distance measurements on photo-excited spin-correlated radical pairs. The correlated radical pair spectrum of $P_{700}^{+\bullet}/A_1^{-\bullet}$ was observed first in 1977 (Blankenship *et al.* 1975). Measurements with high spectral resolution, performed at K-band (24 GHz) and room temperature (Bock *et al.* 1988) and later also at W-band (95 GHz) (Est *et al.* 1997), allowed to deduce the distance and relative orientation of these two cofactors. The zero-quantum coherence created by the dipolar coupling of the spins after the fast charge separation was observed for the first time in 1991 (Kothe *et al.* 1991). This method has been extended later to Q-band frequencies (34 GHz) leading to a higher spectral resolution (Link *et al.* 2001). Out-of-phase echo modulation

was seen for the first time on PS I of cyanobacteria (Thurnauer & Clark, 1984). Later on, this method was used to compare the structure of the radical pair in PS I and bRC (Bittl & Zech, 1997) and mutants thereof (Santabarbara *et al.* 2005).

4.2.3.3 Photosystem II

Examples for out-of-phase echo measurements on PS II are two studies of Hara *et al.* (1997) and Zech *et al.* (1997) on the radical pair $P_{680}^{+\bullet}/\ Q_A^{-\bullet}$, yielding distances of 27·2 and 27·4 Å, respectively. Interestingly, the latter study was performed at physiological temperatures. Low temperature measurements on oriented membranes revealed an angle of 21° between the dipolar vector and the membrane normal (Yoshii *et al.* 1999a). Out-of-phase echo measurements have also been applied to acquire the distance between $Q_A^{-\bullet}$ and $Y_Z^{+\bullet}$ (Zech *et al.* 1999). This distance was later confirmed by PELDOR ($R = 34{\cdot}5 \pm 1$ Å) (Kawamori *et al.* 2002) and by the X-ray structure with $R = 34{\cdot}2$ Å (Zouni *et al.* 2001). A spin-polarized radical pair constituted out of a triplet chlorophyll (^{3}Chl) and $Q_A^{-\bullet}$ displayed in the out-of-phase echo modulation an oscillation with a frequency corresponding to $25{\cdot}9 \pm 0{\cdot}5$ Å. The authors suggested that this ^{3}Chl signal originates from the accessory chlorophyll on the D1 protein by comparison with X-ray data (Kawamori *et al.* 2005).

While for the out-of-phase echo modulation spin-polarized radical pairs are essential, the '2 + 1' echo sequence and PELDOR are applicable to trapped non-polarized radical pairs. In such experiments, $Y_D^{+\bullet}$ was frequently used as one spin center and its distances to other cofactors was measured. For the $Y_D^{+\bullet}/\ Y_Z^{+\bullet}$ pair a distance of $29{\cdot}5 \pm 0{\cdot}5$ Å (Astashkin *et al.* 1994) and an angle between the distance vector and membrane normal of 80° or 100° was found (Astashkin *et al.* 1998). The distance was later reconfirmed (Tonaka *et al.* 2000) and agrees with the distance in the X-ray structure ($r = 29{\cdot}2$ Å). For the couple $Y_D^{+\bullet}/Chl\ Z^{+\bullet}$ a distance of $29{\cdot}4 \pm 0{\cdot}5$ Å (Shigemori *et al.* 1998) and an orientation with respect to the membrane normal of $50 \pm 5°$ was obtained (Kawamori *et al.* 2002). Both, distance and angle, have been verified recently by PELDOR measurements (Kawamori *et al.* 2005). However, the crystal structure reveals a slightly shorter distance of 26·8 Å. The distance between $Y_D^{+\bullet}$ and $Q_A^{-\bullet}$ was determined to $38{\cdot}5 \pm 0{\cdot}8$ Å, close to the distance of 40 Å found in the crystal structure (Yoshii *et al.* 1999b). Measurements in oriented membranes gave an angle of $13 \pm 4°$ between the dipolar vector and membrane normal (see Fig. 11). PELDOR-based distance measurements are also reported for $Y_D^{+\bullet}$ and a radical species belonging to the so-called doublet signal (Mino *et al.* 2000).

4.3 DNA/RNA

EPR spectroscopic studies on RNA or DNA date back to the 1970s, but were mainly restricted to the analysis of global or sequence dependent mobility of oligonucleotides (Robinson & Drobny, 1995; Robinson *et al.* 1997; Keyes & Bobst, 1998; Liang *et al.* 2000; Qin *et al.* 2001; Qin & Dieckmann, 2004). Only recently, several groups started to employ EPR-based distance measurements between nitroxides to predict structure elements in RNA/DNA. One reason might be that strategies had to be developed first to site specifically spin label oligonucleotides in high yields (Verma & Eckstein, 1998). Another reason is that only during the last 10–20 years, more and more of the structural and functional diversity of RNA has been discovered, making it an increasingly interesting target for studies concerning structure–function relationships and drug targeting.

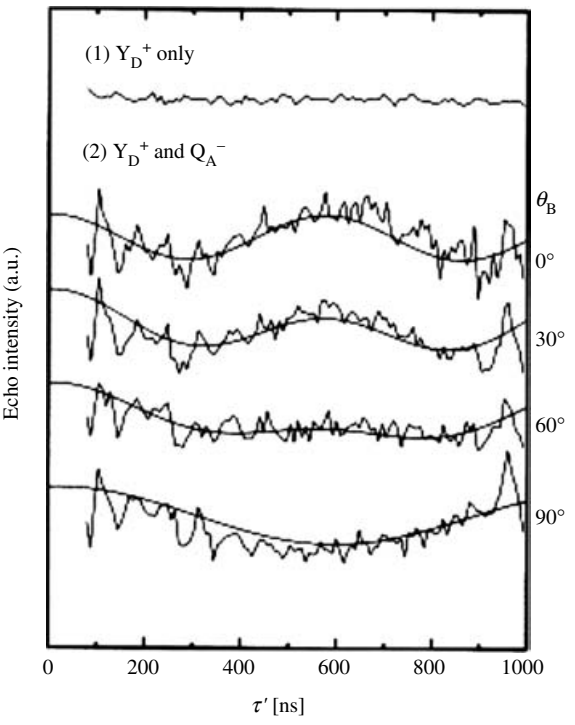

Fig. 11. Out-of-phase echo detection for the couple $Y_D^{+\bullet}/Q_A^{-\bullet}$ in Fe^{2+}-depleted PS II using oriented membranes. Trace 1 shows the time trace for the $Y_D^{+\bullet}$ only case with the membrane normal parallel to B_0 ($\theta_B = 0$). Traces 2 show the variation of the frequency of the modulation for different angles θ_B. The solid lines are simulations (Yoshii *et al.* 1999b).

4.3.1 Spin labeling of DNA/RNA

The methods nowadays available for site-specific spin labeling of oligonucleotides can be divided into three categories: (1) labeling of naturally occurring unique groups, (2) introducing unique groups by means of automated solid-phase synthesis, and (3) enzymatic labeling. Naturally occurring unique groups that can be labeled selectively are the 3′- or 5′-ends (Caron & Dugas, 1976; Luoma *et al.* 1982) or unusual bases within tRNAs, e.g. 4-thiouridine (Hara *et al.* 1970; McIntosh *et al.* 1973). In the former case, labeling is restricted to the ends of oligonucleotides and the latter case is mainly applicable to tRNAs. However, both can be applied to large oligonucleotides. The largest flexibility with respect to labeling sites and labels is given if the oligonucleotide is not longer than $\sim$80 bases. In this case, various protocols exist to introduce nitroxide spin labels to the phosphate backbone, the sugar or the base moiety utilizing automated solid-phase synthesis. The general idea is that a phosphoramidite with a unique functional group is incorporated into the RNA/DNA sequence at the desired position. This group can already be a spin label or a functional group which reacts selectively with a spin label possessing a complementary functional group. Examples are given together with the respective distance measurements in the next section. Especially, Bobst *et al.* showed that the length restriction can be circumvented by enzymatic labeling using Klenow filling (Bobst *et al.* 1988; Keyes & Bobst, 1998); another example is presented by Sprinzl *et al.* (1974). Another possibility might be to ligate two already labeled oligonucleotides by means of a ligase.

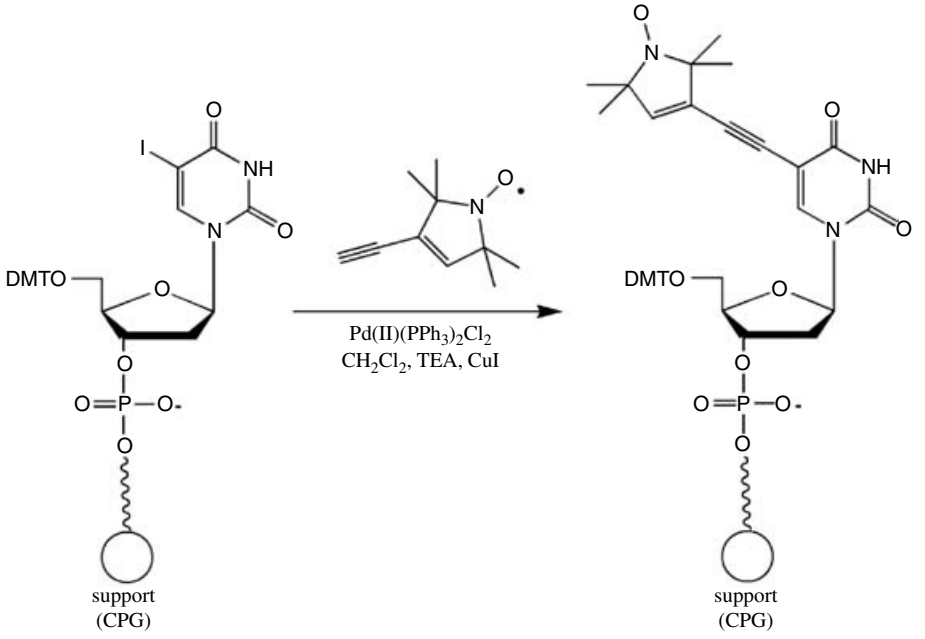

Fig. 12. Spin labeling of RNA/DNA on solid support using TPA (Schiemann *et al.* 2004).

The choice of the appropriate spin label strategy depends on the scientific question and the system under study. To increase the number of accessible systems, easier synthesis strategies with higher yields and different spin labels are needed. For example, very rigid nitroxides attached via two bonds (Miller *et al.* 1995; Okonogi *et al.* 2000; Cekan & Sigurdsson, 2005) could allow gathering of not only information about nitroxide–nitroxide distances, but also about their relative orientation. Spin labels with different combinations of isotopes or other labels than nitroxides could permit individual microwave addressing of each spin center, which is of interest for the analysis of complexes containing more than two labels.

4.3.2 Distance measurements on duplex DNA/RNA

As long as the label does not disturb the structure of the oligonucleotide or its binding to a protein, distance measurements demand rigid and short labels to simplify the translation of distances into structure and allow the observation of deep dipolar oscillations in the case of '2+1', PELDOR, and DQC-EPR. One example is the ethynyl functionalized nitroxide called TPA (see Fig. 12), which is cross-coupled to 5-iodouridine or 5-iodo-2′-desoxyuridine during the automated solid-phase synthesis of RNA (Piton *et al.* 2005; Piton *et al.* 2007) or DNA (Strube *et al.* 2001), respectively. The palladium catalyzed Sonogashira cross-coupling is almost quantitative (>95%), small amounts of spin label are required, the 5-iodouridinephosphoramidites are commercially available, and the overall yield of doubly spin-labeled RNA/DNA is high (35–50% on a 0·2-μM scale) (Schiemann *et al.* 2007). Another synthetically more challenging way is to synthesize the TPA-labeled phosphoramidite and to incorporate it into the oligonucleotide (Spaltenstein *et al.* 1989). PELDOR measurements were performed on several doubly TPA-labeled DNA (Schiemann *et al.* 2004) and RNA (Piton *et al.* 2007) duplexes with different distances between the two labels (see Fig. 13). All of the PELDOR time traces show at least one full

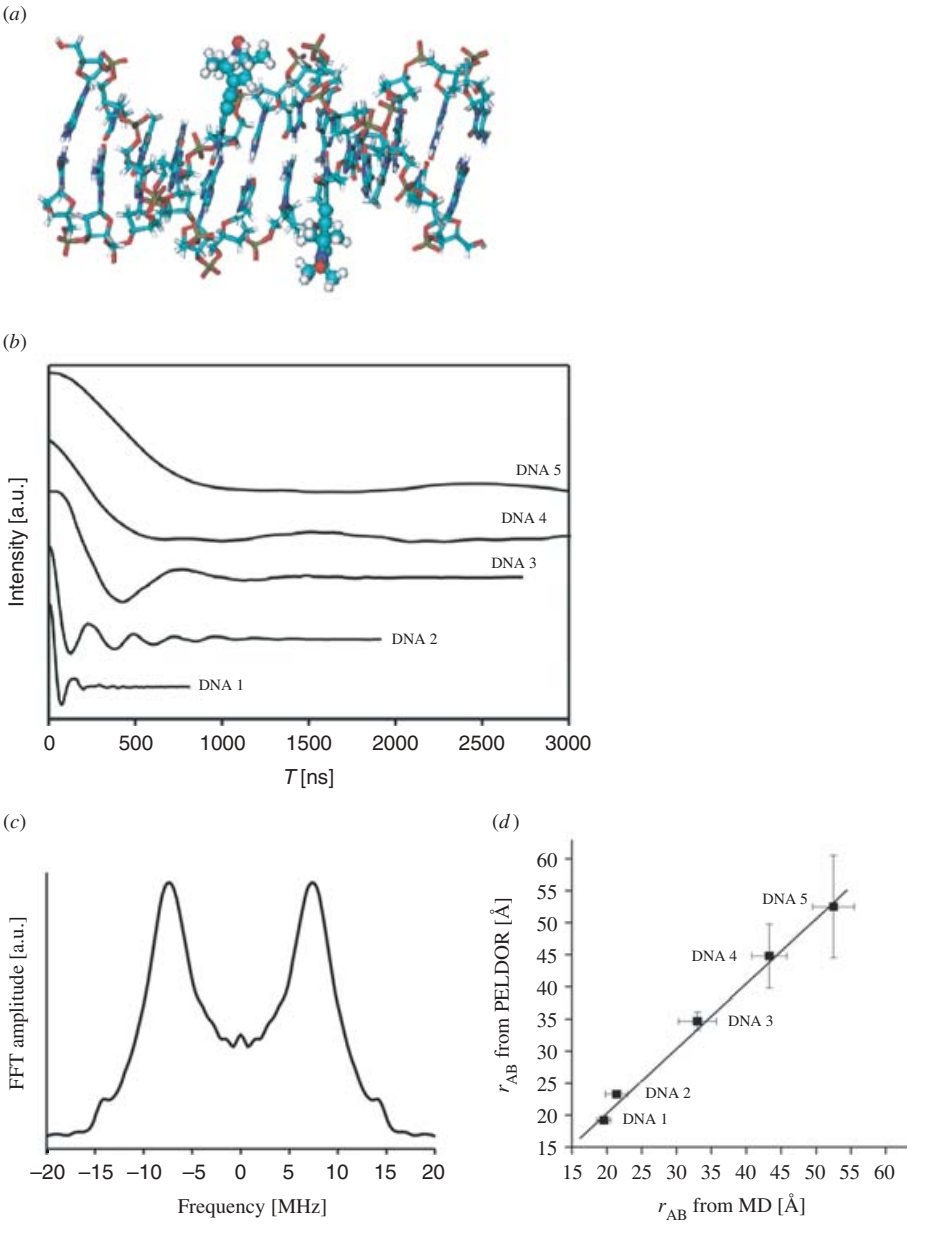

Fig. 13. PELDOR based distance ruler for DNA. (*a*) Structure of two-fold TPA labeled DNA as obtained from MD-simulations. (*b*) PELDOR time traces of five DNAs with increasing distance between the TPA labels. The intermolecular background was subtracted. (*c*) Pake pattern achieved by Fourier transformation of the PELDOR time trace of DNA 1. (*d*) Correlation between the distances gathered from PELDOR and those from MD simulations (Schiemann *et al.* 2004).

oscillation period allowing to establish a reliable and precise nanometer distance ruler for oligonucleotides stretching from 15 to 55 Å. MD simulations on the labeled oligonucleotides were then used to correlate the obtained distances with the DNA/RNA structure. This confirmed that DNA and RNA duplexes retain their B- and A-forms, respectively, in frozen

buffer solution and the presence of 20% ethylene glycol. For a detailed description of the setup of the PELDOR experiment and the spin labeling of oligonucleotides with TPA refer to Schiemann *et al.* (2007).

The group of Sigurdsson published in 2001, a method by which a nitroxide is attached to the 2′-sugar site of RNA strands via a urea linker (Edwards *et al.* 2001). This protocol is limited to the 2′-sugar site and the linker is more flexible than the ethynyl group, but the commercial availability of the 2′-amino-uridinephosphoramidite, the easy one-step synthesis of the functionalized spin label and the straight forward coupling step are advantageous. PELDOR spectra of a RNA duplex labeled with two of these nitroxides show a weak modulation amplitude, but the frequency of the oscillation fits nicely to the distance of 35 Å expected from structure modeling (Schiemann *et al.* 2003). The weak modulation amplitude may be traced back to the larger flexibility of the nitroxide linker and/or to the fact that these experiments were performed without ethylene glycol.

DeRose and colleagues use instead of the isocyanate nitroxide a succinimidyl-functionalized label and couple it to 2′-amino-modified RNA (Bowman *et al.* 2004). The resulting amide group is as short as the ethynyl group, but the conformational degree of freedom is larger and coupling yields are very low. PELDOR experiments with time traces as short as 700 ns on two such duplex RNAs show in one case a weak oscillation corresponding to the predicted distance of 24 Å, whereas the other one does not show any modulations. Tikhonov regularization of the latter time trace exhibits a peak between 16 and 20 Å close to the modeled distance but in addition several broad peaks of less intensity, which are attributed to inter-duplex distances resulting from end-to-end stacking of duplexes. The same group used Fourier deconvolution of dipolar broadened continuous wave EPR spectra to establish a RNA ruler in the range of 5–20 Å (Kim *et al.* 2004).

Recently, a spin labeling method was published in order to label the phosphate backbone of DNA by coupling an iodomethylnitroxide to phosphorothiolates (Qin *et al.* 2001). A similar strategy has been used by Nagahara *et al.* (1992). The big advantage of these methods is their sequence independence; disadvantages are the occurrence of R_P and S_P stereoisomers and that the nucleotide in the 5′-direction has to be substituted by a desoxyribonucleotide to avoid RNA strand cleavage. If both the isomers are separated, yields decrease by 50%, if they are not separated, distance distributions are broadened. Nevertheless, PELDOR measurements ranging from 20 to 40 Å on a set of doubly labeled dodecamer DNA duplexes showed nice agreement with structural models based on NMR data and generic B-form DNA (Cai *et al.* 2006). This study also confirmed that the B-form of DNA is retained upon freezing. Furthermore, in all of the cases discussed above UV–VIS melting studies, CD measurements, and/or MD simulations indicate only minor and local effects of the labels on the duplex structure. An independent MD analysis of TPA and of a six-membered ring analog (Gannett *et al.* 2002) attached to DNA duplexes indicated structural disturbances which are slightly larger and not local (Darian & Gannett, 2005), but the sampling times of the MD simulations were only 4 ns and might not have reached thermodynamic equilibrium yet. Interestingly, it was found that the measured and modeled spin–spin distances all agree well, whereas the distance distributions show differences (Cai *et al.* 2006). We observed a similar trend in our studies (unpublished data). This effect may be caused by a too short MD sampling time, which excludes, for example, RNA/DNA bending or differences between the frozen and liquid state.

The longest distance measured by all EPR methods in a biomolecule so far amounts to 72 Å (Borbat *et al.* 2004). This was accomplished by employing DQC-EPR and a 26 bp long RNA duplex labeled at the ends with an iodacetamide nitroxide attached to 4-thiouridine. The spin

labeling strategy works also within RNA/DNA sequences (Ramos & Varani, 1998) or with MTSSL (Qin *et al.* 2003), is practically easy to handle, and the nitroxide as well as the 4-thiouridine phosphoramidite are commercially available. A major drawback is that the uridine base 'loses' its N3 imino hydrogen upon labeling, which can lead to large, global structural perturbations.

4.3.3 Distance measurements on biologically relevant DNA/RNA

Summarizing the results from the previous section, it is obvious that several strategies are nowadays available for RNA/DNA spin labeling and that EPR spectroscopy is a powerful tool to measure precisely and reliably distances in oligonucleotides in the range from 5 to 75 Å. Nevertheless, applications of this method to biological relevant oligonucleotides or oligonucleotide/protein complexes are rare and mainly restricted to continuous wave EPR methods.

The DeRose group published a study related to Ca^{2+}-induced structural changes in the HIV-1 TAR RNA in 2004 (Kim *et al.* 2004). They labeled uridines 25 and 40 located within the bulge region of TAR and determined the interspin distance in the presence and absence of Ca^{2+} by Fourier deconvolution of continuous wave EPR spectra. The obtained distances of 14·2 and 11·9 Å are close to the modeled distance and show the anticipated increase in distance upon Ca^{2+} binding. Earlier in 1999, a continuous wave EPR distance measurement on the HIV Rev peptide complex binding to the Rev response element (RRE) RNA was reported (Macosko *et al.* 1999). The RNA was labeled by incorporating a guanosine monophosphorothioate at the 5′-end using T7 RNA polymerase and subsequent reaction of the thioate group with MTSSL. By displacing the 5′-end, three different RNA constructs were prepared. The second MTSSL label was introduced into the peptide. Continuous wave EPR spectra of two of these complexes showed dipolar line broadening upon complex formation. Fourier deconvolution yielded distances of 12 and 14 Å in agreement with NMR structures of the complex. The third complex did not show any line broadening, which was expected due to the distance of 40 Å predicted from the NMR structure. Bowman *et al.* (2005) used PELDOR to estimate the spatial distribution of radicals in tracks of heavy atom irradiated DNA.

4.4 Metal centers in proteins

4.4.1 Continuous wave EPR

Continuous wave EPR-based distance measurements between metal centers are hampered by the broad inhomogeneous line width and are thus restricted to fairly short distances (Eaton & Eaton, 2002). The dipolar splitting of the di-copper substituted aminopeptidase from *Aeromonas proteolytica* is resolved at X-band and a copper–copper distance of 5 Å was calculated from the spectra using simulations (Bennett *et al.* 2002). Interestingly, the di-copper substituted enzyme is catalytically more active than the native di-zinc enzyme for which the crystal structure revealed a metal-to-metal distance of 3·5 Å. An example for the potency of continuous wave high-field EPR is the resolution of a dipolar coupling between the Mn^{2+}-ion and the binuclear mixed-valent Cu_A-center in cytochrome *c* oxidase at 95 GHz (Käss *et al.* 2000). In this case, the dipolar coupling led to a splitting of each manganese lines into doublets, which is impossible to observe at X-band frequencies (see Fig. 14). If the Cu_A-center is reduced to a diamagnetic state, the splitting disappears, which proves that the splitting is caused by an electron–electron interaction. A distance of 9·4 Å was extracted by simulations. In the case of smaller distances like in the

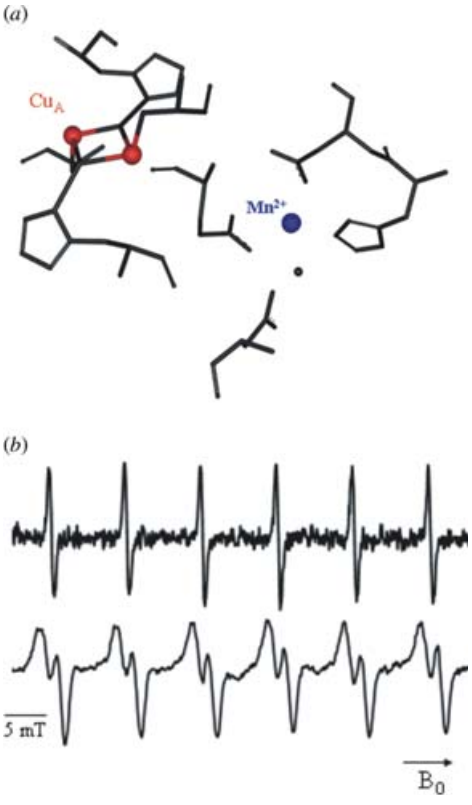

Fig. 14. Dipolar splitting observed by high-field continuous wave EPR spectroscopy. (*a*) Crystal structure of the metal(II) binding site in cytochrome *c* oxidase of *Paracoccus denitrificans* (Ostermeier *et al.* 1997). (*b*) Continuous wave W-band EPR spectra of the Mn^{2+} ion with the Cu_A site reduced (top) and oxidized (bottom). The splitting is well-resolved on each Mn^{2+}-line in the oxidized case (Käss *et al.* 2000).

dimanganese(II,II) catalase from *Thermus thermophilus* or in the arginase from rat liver, where R amounts to ∼3·5 Å (Khangulov *et al.* 1995), the dipolar coupling between two Mn^{2+}-ions can also be estimated by simulations of continuous wave X-band EPR spectra (Golombek & Hendrich, 2003). However, more reliable results are obtained by measuring Mn^{2+}-ions at higher fields/frequencies (Ubbink *et al.* 2002).

4.4.2 PELDOR

Pulsed-EPR based distance measurements involving metal centers are more demanding than those between organic radicals. One reason is that the spectra can extend over a broad spectral range, leading only to partial excitation and thus weak modulation amplitudes and strong orientation selections. Spin states higher than $\frac{1}{2}$ and fast relaxation times further complicate the experiment.

4.4.2.1 Metal/metal

The first PELDOR measurement between two metal sites has been reported by Elsässer *et al.* (2002) for the [NiFe]-hydrogenase from *Desulfovibrio vulgaris Miyazaki F*. The metal sites are the

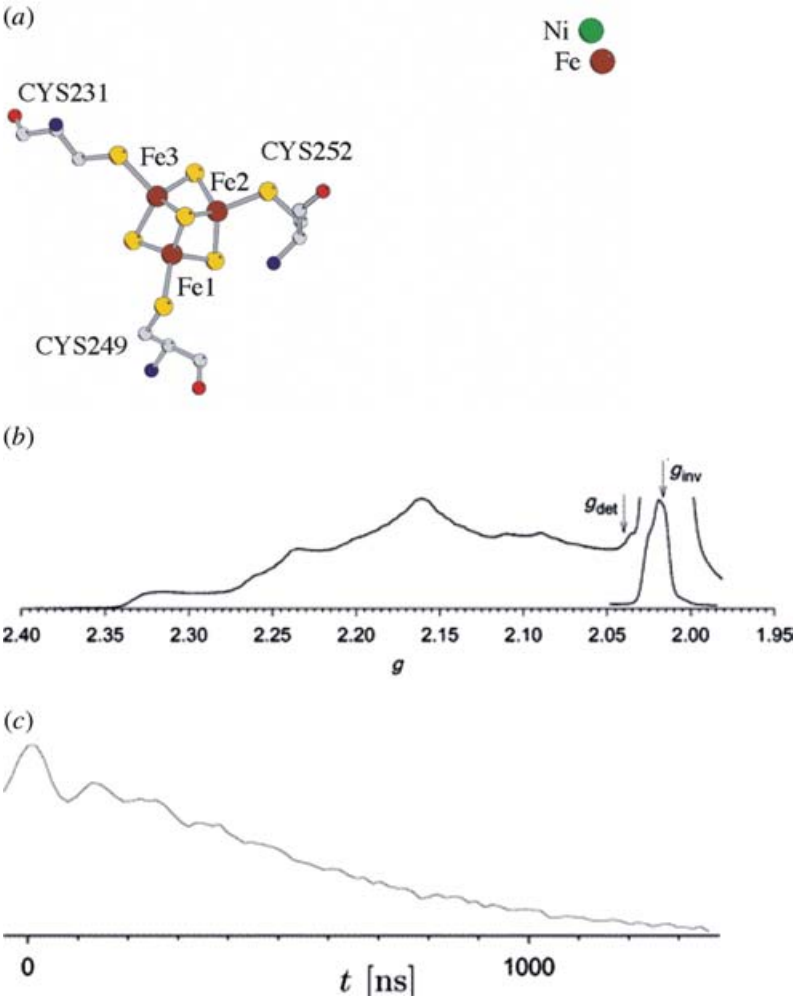

Fig. 15. PELDOR measurements between two metal sites. (*a*) Structure and arrangement of the [NiFe]- and the [3Fe–4S]$^{+}$-cluster in the [NiFe]-hydrogenase from *Desulfovibrio vulgaris Miyazaki F* [PDB (http://www.rcsb.org) entry 1H2A]. (*b*) Two-pulse field-swept echo EPR spectrum of the hydrogenase. (*c*) PELDOR time trace with the detection sequence applied on the [NiFe] center and the inversion pulse on the strong [3Fe–4S]$^{+}$-signal (Elsässer *et al.* 2002).

[NiFe]- and the [3Fe–4S]$^{+}$-cluster both with an effective spin of $S=\frac{1}{2}$. The PELDOR time traces were recorded at 5 K in order to slow down relaxation and resolve dipolar modulations (see Fig. 15). The deepest modulation was observed by detecting the [NiFe] signal and inverting parts of the [3Fe–4S]$^{+}$ signal. The frequency of the observed oscillation (8·5 MHz = 18 Å) does, however, not correspond to the average distance of 21 Å inquired from the X-ray structure. The authors solved this discrepancy by weighting the individual distance between each iron in the [3Fe–4S]$^{+}$ cluster and the [NiFe] center by the individual spin projection factors. The spin projection factors within the cluster were known from Mössbauer studies, but could not be assigned to individual iron ions. For the [NiFe] center it was known that the spin is localized on the nickel center. Thus, the authors used the distance found in the crystal structure and assigned

the spin projection factors by fitting the PELDOR data. Excellent agreement was achieved when the largest spin projection factor was ascribed to the iron ion closest to the [NiFe] center. In general, spin projection factors are to be considered in cases of spin delocalization or coupling of spins on different atoms to an effective total spin. The effect of orientation selection was discussed in detail by the same authors (Elsässer *et al.* 2005).

One year later, PELDOR measurements on a covalently linked azurin dimer containing two Cu^{2+}ions ($S=\frac{1}{2}$) were reported (Amsterdam *et al.* 2003). The time trace shows an oscillation corresponding to a distance of 26 Å. In contrast, tethering two azurins via a flexible linker did not yield an oscillation, which has been explained to the expected short distance of 14 Å, but may also be due to a large distance distribution caused by the flexible linker. DQC-EPR was performed to measure a Cu^{2+}–Cu^{2+} distance in a model peptide (Becker & Saxena, 2005). However, the double quantum coherence pathway could not be effectively filtered from the single quantum pathways containing the hyperfine modulations due to the spectral width of the Cu^{2+} spectrum. Attempts to measure the Mo^{5+}–Fe^{3+} distance in sulfite oxidase by means of PELDOR did not reveal any dipolar oscillations (Codd *et al.* 2002).

4.4.2.2 Metal/organic cofactor

PELDOR experiments with deep oscillations involving the oxygen-evolving manganese cluster (OEC) of PS II were performed in 1996, yielding a distance of $27 \pm 0{\cdot}2$ Å between the manganese cluster in the S_2 state ($S=\frac{1}{2}$) and the tyrosin D cation radical ($Y_D^{+\bullet}$) (Hara *et al.* 1996). One year later, orientation selective PELDOR measurements have been reported on the same system in oriented membranes (Astashkin *et al.* 1998). These experiments confirmed the distance previously obtained and provided in addition an angle of $110^\circ \pm 2^\circ$ between the membrane normal and the distance vector connecting the manganese cluster with $Y_D^{+\bullet}$.

In contrast, a PELDOR measurement between $Y_D^{+\bullet}$ and the manganese cluster in the S_0 state gave a distance of 34 ± 1 Å (Arao *et al.* 2002). This distance is 7 Å larger than found for the manganese cluster in the S_2 state and both distances deviate from the distance of 30·3 Å found in the X-ray structure (Zouni *et al.* 2001). The reason for these discrepancies is most likely the failure of the point-dipole approximation used for the interpretation of the PELDOR time traces. In the case of clusters, the spin–spin coupling between the constituting metal ions have to be dealt with explicitly. These spin–spin couplings and therefore the spin projection factors change by switching the cluster from the S_2 to the S_0 state, leading to different distances for both states (Bittl & Kawamori, 2005).

PELDOR was also applied in order to measure the distance between $Q_A^{-\bullet}$ in PS II and the heme Fe^{3+} located between the two subunits of cytochrome b_{559} (Kuroiwa *et al.* 2000). Cytochrome b_{559} is a small electron carrier protein that binds to PS II and is involved in several side-reactions of PS II. Because the EPR spectrum of the heme iron is broad, orientation selective measurements at X-band were possible. Performing these experiments in oriented and nonoriented membranes led to a Fe^{3+}–$Q_A^{-\bullet}$ distance of 40 Å and additionally an angle of 78° between the dipolar distance vector and the membrane normal. The X-ray structure revealed a larger distance of 47·8 Å (Zouni *et al.* 2001). The distance to $Y_D^{+\bullet}$ on the other site of PS II could not be resolved, probably due to the expected large distance of 50 Å. Such a distance corresponds to an oscillation period of about 2400 ns, which exceeds the experimental time window of 1400 ns.

4.4.3 Relaxation methods

In cases where a slowly relaxing spin is coupled to a fast relaxing spin, distances can be calculated from the relaxation enhancement detected on the slowly relaxing spin. The quantitative analysis of such data requires the knowledge of several parameters as outlined in Sections 2.6.1 and 2.6.2. It is, however, worth the effort in cases where PELDOR fails due to a broad spectral width, fast T_2 of the observer spin or a too fast T_1 of the pumped spin.

4.4.3.1 Metal/metal

Examples for relaxation measurements involving two metal sites are the three studies on the mixed-valent, binuclear Cu_A-center ($S=\frac{1}{2}$), and the cytochrome *a* (Fe^{3+}, $S=\frac{1}{2}$) in cytochrome *c* oxidase prior to the crystal structure ($R_{Cu_A-Fe^{3+}}=19{\cdot}5$ Å; Ostermeier *et al.* 1997). In one case, a distance of 13–26 Å has been extracted from temperature dependent continuous wave EPR saturation data, which contain the product of T_1 and T_2 (Brudvig *et al.* 1984). In contrast, measuring the relaxation enhancement on T_1 using pulsed saturation recovery led to an upper distance of 10 Å (Scholes *et al.* 1984). In the third case, a lower limit of 8 Å and an upper limit of 13 Å has been found using progressive power saturation, which depends on the product of T_1 and T_2 (Goodman *et al.* 1985). These discrepancies may be due to the concurrent presence of several coupled spin centers.

The detailed study on succinate:ubiquinone reductase from *Paracoccus denitrificans* (Hung *et al.* 2000) is exemplary in its detailed analysis. In this system, a [3Fe–4S] cluster with a total spin of $S=\frac{1}{2}$ is the slow relaxing spin center and a Fe^{3+} ion (*b*-heme, $S=\frac{1}{2}$) is the fast relaxing spin. The relaxation enhancement was measured on T_1 of the iron–sulphur cluster by means of inversion recovery and 'picket-fence' pulse sequences in a temperature range of 4–8 K. The 'picket-fence' sequence has the advantage of excluding spectral diffusion artifacts from the time trace. A distance of $R \geqslant 10$ Å between both metal centers was obtained from an analysis including relative orientations. Recently, T_2 Hahn-echo measurements have been used to assess the distance between cytochrome *c* and cytochrome *c* oxidase in the cytochrome *c*/cytochrome *c* oxidase complex (Lyubenova, 2007).

4.4.3.2 Metal/organic cofactor in PS II

Relaxation enhancement on $Y_D^{+\bullet}$ in PS II due to coupling to the manganese cluster in the S_2 state was measured via spin diffusion, using an electron spin echo method employing selective hole burning with subsequent detection of the hole broadening (Kodera *et al.* 1994). The obtained distance of $\sim$28 Å is in good agreement with PELDOR data (Hara *et al.* 1996) and another relaxation study which includes also the S_1-state (Mamedov *et al.* 2004). The distance discrepancy with respect to the crystal structure might again be due to the use of the point-dipole approximation. Relaxation enhancement on $Y_D^{+\bullet}$ has also been utilized to determine its distance to the nonheme iron in PS II. Temperature dependent T_1 measurements using saturation recovery yielded a distance of 38 ± 5 Å (Hirsh *et al.* 1992) in agreement with selective hole burning, $R=42 \pm 2$ Å (Kodera *et al.* 1994) and saturation EPR at high field, 40 Å (Un *et al.* 1994).

Distances from the non-heme iron to a β-carotene and to a monomeric chlorophyll have been extracted both by using a three-pulse echo-detected saturation recovery sequence (Lakshmi *et al.* 2003). The experiments were performed at a microwave frequency of 130 GHz to resolve the EPR spectra of both cofactors (see Fig. 16). A saturation pulse length of 10 ms was used to measure the relaxation enhancement on T_1 without spin diffusion contributions. The analysis

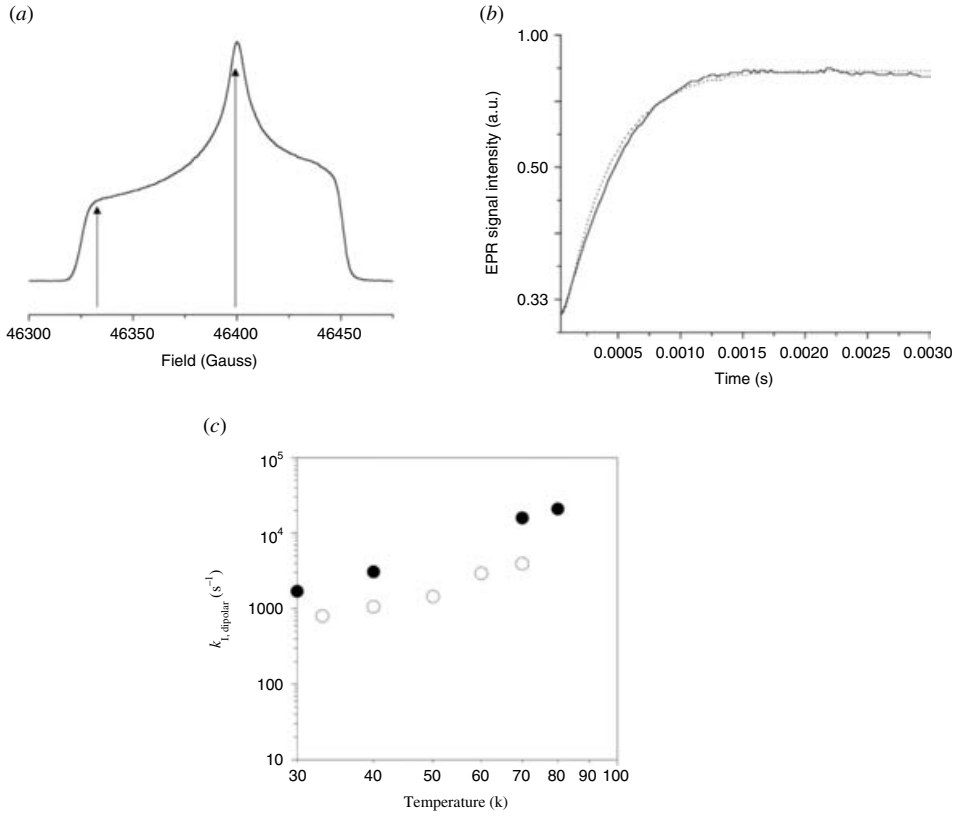

Fig. 16. Distance determination via relaxation enhancement. (*a*) 130 GHz two-pulse Hahn-echo detected field-swept spectrum of $Y_D^{+\bullet}$ in PSII. The arrows indicate two different field positions at which saturation recovery experiments were performed. (*b*) The obtained saturation-recovery traces at the two field positions (low field = solid line and high-field = dashed line). The slightly different relaxation times may indicate relaxation anisotropy. (*c*) Dipolar relaxation rates extracted from measurements at different temperatures and at D-(filled circles) and X-band (open circles). The analysis of relaxation data collected at various temperatures and different frequencies allowed to obtain a unique solution (Hirsh *et al.* 1992; Lakshmi *et al.* 2003).

included spin density distributions and yielded distances of 38 Å and $\geqslant 40$ Å from the iron to the β-carotene and the chlorophyll radical, respectively, The distance of the nonheme iron to the pheophytin radical was estimated to 20 ± 4 Å based on temperature-dependent pulsed EPR measurements of T_1 (Deligiannakis & Rutherford, 1996). Distances measured between the manganese cluster and $Y_Z^{+\bullet}$ or $P680^{+\bullet}$ using various approaches are inconsistent, as discussed by Bittl & Kawamori (2005).

4.4.3.3 Metal/nitroxide

A ruler comprised out of a copper–histidine complex attached to the N-terminus of the long interdomain helix of T4 lysozyme and a nitroxide coupled to three different positions on this helix was reported in 1995 (Voss *et al.* 1995a, b). The relaxation enhancement was extracted from continuous wave EPR spectra by comparing the line intensity of the dipolar coupled copper–nitroxide system with the intensity of the same line in the absence of copper. This method is applicable in the range of 10–25 Å at cryogenic and more important also at

room temperature. This approach was also applied later on to the lactose permease of *E. coli* (Voss *et al.* 1995a, b, 1998). It should, however, be kept in mind that in this case the product of T_1 and T_2 is determined and that both relaxation times have to be known to yield reliable distances.

Recently, the unfolding of alanine-based peptides was observed via relaxation enhancement in the liquid state ($T = 270$–315 K) (Jun *et al.* 2006). The peptides were labeled with a copper complex and a nitroxide. The relaxation enhancement was measured on the longitudinal relaxation time T_1 of the nitroxide by means of a FID detected inversion recovery experiment. Detection via the FID was necessary due to the fast transverse relaxation time of the nitroxide at this temperature. It was also attempted to localize the metal(II) binding site in the 16-kDa proton channel of *Nephrops norvegicus* (Páli *et al.* 2006) in the liquid state. Here, the endogenous Cu^{2+} was exchanged for the faster relaxing Ni^{2+} and nitroxides were attached to the membrane or to the proteolipid itself. The relaxation enhancement was measured on T_1 by means of saturation transfer EPR (Marsh & Horvath, 1989). The found distances were in the range of 14–23 Å and do agree with a structural model. In 2004, a computational method to localize a slow relaxing spin buried in a protein was reported. The relaxation enhancement was induced by adding relaxation-enhancing agents like Dy^{3+} complexes to the solution (MacArthur & Brudvig, 2004). Further examples concerning distance measurements to metal centers via relaxation enhancement or by other methods are summarized by Berliner *et al.* (2000).

4.5 Multiple spin centers

As discussed in Section 2.3.2, PELDOR can not only be used to measure the distance between two spin centers, but also to count the number of interacting spin centers. This can, for example, be utilized to determine the number of monomers constituting aggregates of biomolecules as pioneered by Milov *et al.* in their work on the antibiotic trichogin GA IV, as described in the next section.

4.5.1 Trichogin GA IV

Trichogin GA IV is a peptide of fungal origin and belongs to the class of peptaibols. It is proposed that trichogin self-assembles in membranes to helix bundles and modifies thereby the surrounding membrane. To verify this hypothesis, one of the α-aminoisobutyric acid (Aib) residues in the trichogin helix was substituted by TOAC (Milov *et al.* 2000). The observation of clear oscillations demonstrated the formation of specific aggregates with fixed distances between the spin labels within a chloroform/toluene mixture. From the modulation depth $V(T \rightarrow \infty)$ of $0{\cdot}51 \pm 0{\cdot}01$ found for the aggregates and a λ of 0·2 calculated from a monomeric but doubly labeled trichogin, the average number of monomers within the aggregates was estimated to be $4{\cdot}0 \pm 0{\cdot}3$. Together with molecular modeling this data were then used to construct a structural model for the trichogin helix bundles. Best agreement was achieved for bundles of four antiparallel aligned helices with a 3_{10}-conformation. The hydrophilic amino side chains point to the inside of the bundle and the hydrophobic side chains extend to the exterior. Addition of ethanol to the solution led in each case to PELDOR time domain data, exhibiting only monoexponential decays without any oscillation, which was interpreted as dissociation of the helix bundles into their constituting monomers.

The 3_{10}-helix conformation was confirmed in a later paper (Milov *et al.* 2001) by mixing small amounts of doubly labeled trichogin with unlabeled trichogin. The observed oscillation with a period of 75 ns corresponds to an intra-trichogin distance of 15·7 Å, close to the expected distance of ∼14 Å for a 3_{10}-helix. The 2_7-helix found for a modified trichogin in chloroform/dimethylsulfoxide (see Section 3.1.1) is probably due to this particular solvent, as a comparative study with various solvent mixtures showed (Milov *et al.* 2004). PELDOR studies on trichogin covalently linked together to yield head-to-tail dimers revealed an α-helical structure in the chloroform/toluene mixture. This change from a 3_{10}-helical structure to an α-helical structure was attributed to the increased length of the peptides. Analysis of the PELDOR modulation depth found for the trichogin dimers indicate that two to three of them form a bundle, depending on the concentration (Milov *et al.* 2003).

Two recent studies of trichogin in multilamellar membranes (Milov *et al.* 2005) and phospholipid bilayers (Salnikov *et al.* 2006) showed, however, that trichogin is monomeric at low peptide/lipid ratios but may dimerize at higher ratios. Under these biologically more relevant conditions, the conformation of the helix seems to be a mixture of α- and extended 3_{10}-helixes. The authors also studied the self-aggregation of the channel forming antibiotics alamethcitin (Milov *et al.* 2006) and zervamicin IIa (Milov *et al.* 2002) by PELDOR.

4.5.2 Other examples

In an EPR study on the Nha A Na^+/H^+ antiporter of *E. coli* in phospholipid membranes, PELDOR spectra without visible modulation, but clearly multi-exponential decay were interpreted as indication for the formation of specific dimers and small pH-induced changes were discussed (Hilger *et al.* 2005). In the case of the von Willebrand Factor A, Tikhonov regularization yielded a distance of 61·5 Å and the authors claim evidence for a trimer which could not be shown unequivocally from the modulation depth (Banham *et al.* 2006). The observation of only one distance was attributed to the formation of a symmetric trimer. Such a symmetric trimer is also found in the crystal structure and the distance between the spin labels modeled into the crystal structure is close to the experimental one.

PELDOR was also applied to analyze the three-spin systems $Y^{\bullet}_{D}$–$Q^{-\bullet}_{A}$–$Y^{\bullet}_{Z}$ and $Chl^{+\bullet}_{Z}$–$Q^{-\bullet}_{A}$–$Y^{\bullet}_{D}$ generated in PS II (Kawamori *et al.* 2003). In both cases the number of coupled spins was not counted, but the oscillations of the PELDOR time traces were used to extract the three distances. In this way, the previously unknown $Chl^{+\bullet}_{Z}$–$Q^{-\bullet}_{A}$ distance could be calculated to $R = 34$ Å and the same distance was obtained for the $Q^{-\bullet}_{A}$–$Y^{\bullet}_{Z}$ pair. The general problem of assigning the measured distances in a multi spin-center system to the actual spin partners might be circumvented by isotope labeling, as shown by Jeschke *et al.* on ^{14}N, ^{15}N-labeled bisnitroxide model systems (Jeschke *et al.* 2006).

5. Comparison of spectroscopic methods

5.1 Comparison of EPR methods

Dipolar oscillations can be observed with PELDOR, DQC-EPR, '2 + 1', out-of-phase echo, and quantum-beat experiments and directly converted into distances. The requirement for the direct conversion is that the whole Pake pattern is observed or that the orientation-dependent term can be determined by orientation-dependent measurements. If the whole Pake pattern or at least

both singularities are resolved, the isotropic exchange coupling constant J can be quantified and separated from ω_{dip}. In this way distances of up to 80 Å are assessable. However, the following limitations have to be considered: The out-of-phase echo experiment can only be applied to photo-excited spin-correlated radical pairs, whereas the other methods can be used for distance measurements on stable or trapped radicals. '2+1' has the disadvantage of strong hyperfine artifacts, which are strongly diminished in PELDOR and DQC-EPR, but the latter two techniques are technically more demanding.

A dipolar coupling for distances smaller than 10 Å is usually visible as a line splitting in continuous wave EPR spectra. Distances up to 20 Å induce dipolar line broadening from which distances can be extracted, but the analysis relies on lineshapes, which decreases the accuracy. Relaxation-based methods are also sensitive to the dipolar coupling strength but rely on the analysis of monotonic decays or lineshapes, which is intrinsically more susceptible to errors than oscillating patterns as obtained from methods with a coherent flip of the B spin. The advantage of relaxation methods and continuous wave EPR methods is that both can be applied to the liquid state at physiological temperatures, whereas pulsed methods usually require cryogenic temperatures to slow down relaxation processes. Furthermore, relaxation measurements may be the only way to extract distances between metal centers with broad spectral width and/or short relaxation times.

5.2 Comparison of EPR with FRET and NMR

FRET (Lakowicz, 2006) and EPR-based methods cover roughly the same distance range. But the following differences occur:

(1) If dipolar oscillations are observed, it is easier to translate these into a distance, than extracting a distance from differences in fluorescence intensities.
(2) If the whole Pake pattern is observed or if the orientation dependence is resolved, no assumptions about orientations have to be made, whereas the orientation factor κ is usually set to 2/3 in FRET.
(3) If the whole Pake pattern is observed, the two coupling mechanisms J and ω_{dip} can be separated from one measurement. In FRET, different mechanisms leading to fluorescence quenching have to be carefully deconvoluted, using standard samples without acceptor, but under otherwise identical conditions or additional measurements. In this sense, FRET, is similar to relaxation-based EPR methods.
(4) The labels used in EPR are usually smaller and more rigid than the chromophores commonly used in FRET, leading to an easier correlation between measured distance and structure of the biomolecule.

On the other hand, FRET has several advantages:

(1) It is generally applicable in liquid solution at room temperature. EPR methods can also be applied to liquids, but then the precision is reduced.
(2) FRET signals can be measured on a single molecule level.
(3) FRET can be used to monitor motions in real time, whereas PELDOR and DQC-EPR demand freeze-quench techniques to get snapshots of the biomolecule in motion.

Several NMR methods exist to measure long-range distances. These are, for example, solid-state NMR methods like REDOR (Gullion & Schaefer, 1989; Gullion & Vega, 2005) or

the recoupling of residual dipolar couplings in liquid-state NMR (Tolman *et al.* 1995; Tjandra *et al.* 1996) using alignment media as, for example, micelles. Yet, due to the smaller magnetic moment of the nuclei the distance range is limited to roughly 20 Å and for measurements in orienting media the order parameter S^2 has to be known. Liquid-state NMR-based paramagnetic relaxation enhancement (PRE) experiments allow to gather longer distances (Donaldson *et al.* 2001; Bonvin *et al.* 2005; Iwahara & Clore, 2006), but the method is less quantitative (Sharp *et al.* 2001). However, this is overcompensated by the simultaneous observation of several NMR signals allowing to collect numerous constraints in one spectrum. On the other hand, NMR is restricted with respect to the size of the biomolecules, whereas FRET and EPR are not. In summary, all these techniques are complementary to each other.

6. Conclusion and outlook

The combination of site-directed spin labeling and pulsed-EPR methods enable to routinely study large biomolecules like peptides, proteins, oligonucleotides, and complexes thereof either in solution or in membranes. It was shown that with some of these methods, distances can be obtained very precisely and parameter free up to 80 Å in frozen solution. Distances can also be obtained in the liquid state, but these results are less precise and restricted to shorter distances. For measurements in frozen solution, dynamics are not directly accessible, but several studies suggested that distance distributions in the frozen state may be correlated with dynamics in the liquid state. The orientation between spin centers can be resolved using high-field/high-frequency spectrometers or orienting media. Additionally, PELDOR can be used to count the number of monomers within an aggregate of biomolecules. To be able to assign the different distances in such aggregates to specific spin pairs, labels with separated resonance frequencies are needed.

It might also be valuable to think about synthesizing new types of spin labels with long relaxation times T_2 at room temperature, because it might allow the application of pulsed-EPR methods like PELDOR or DQC-EPR at room temperature in liquid solution. If this were achieved, movements of subunits or folding events could be followed down to microseconds in real time.

7. Acknowledgments

We are grateful to Dr Marina Bennati, Bela Bode, Charlotte Börner, Dr Burkhard Endeward, Dr Jörg Fritscher, Dr Melanie Hertel, Dr Sevdalina Lyubenova, Dominik Margraf, and Dr Jörn Plackmeyer for carefully reading the manuscript. We thank Dr Nelly Piton and Professor Joachim W. Engels as well as Dr Yuguang Mu and Professor Gerhard Stock for their cooperation on the RNA DNA projects and for providing Figs 12 and 13*a*, respectively, Dr Marina Bennati and Dr Vasyl Denysenkov, are thanked for donating Fig. 10, and Professor Hanno Käss and Professor Bernd Ludwig for contributing Fig. 14. We specially thank Bela Bode, Dominik Margraf, and Dr Jörn Plackmeyer for their work related to Fig. 4 and for preparing the figure itself. The financial support of the DFG (SFBs 579 and 472 and SPP 1051), the Biological Magnetic Resonance Center, and the state of Hesse is gratefully acknowledged.

8. References

Altenbach, C., Marti, T., Khorana, H. G. & Hubbell, W. L. (1990). Transmembrane protein structure: spin labeling of bacteriorhodopsin mutants. *Science* **248**, 1088–1092.

Altenbach, C., Oh, K.-J., Trabanino, R. J., Hideg, K. & Hubbell, W. L. (2001). Estimation of inter-residue distances in spin labeled proteins at physiological temperatures: experimental strategies and practical limitations. *Biochemistry* **40**, 15471–15482.

Amsterdam, I. M. C. V., Ubbink, M., Canters, G. W. & Huber, M. (2003). Measurement of a Cu–Cu distance of 26 Å by a pulsed EPR method. *Angewandte Chemie International Edition* **42**, 62–64.

Anderson, D. J., Hanson, P., McNulty, J., Millhauser, G., Monaco, V., Formaggio, F., Crisma, M. & Toniolo, C. (1999). Solution structures of TOAC-labeled trichogin GA IV peptides from allowed ($g=2$) and half-field electron spin resonance. *Journal of the American Chemical Society* **121**, 6919–6927.

Arao, S., Yamada, S., Kawamori, A., Shen, J.-R., Ionnidis, N. & Petrouleas, V. (2002). EPR studies of manganese spin centers in the even number oxidation states of water oxidizing complex of photosystem II. In *EPR in the 21st Century: Basics and Applications to Material, Life and Earth Science* (ed. H. Ohta), pp. 466–470. Amsterdam: Elsevier Science BV.

Astashkin, A. V., Hara, H. & Kawamori, A. (1998). The pulsed electron–electron double resonance and '2+1' electron spin echo study of the oriented oxygen-evolving and Mn-depleted preparations of photosystem II. *Journal of Chemical Physics* **108**, 3805–3812.

Astashkin, A. V., Kodera, Y. & Kawamori, A. (1994). Distance between tyrosines Z^+ and D^+ in plant photosystem II as determined by pulsed EPR. *Biochimica et Biophysica Acta* **1187**, 89–93.

Ban, N., Nissen, P., Hansen, J., Moore, P. B. & Steitz, T. A. (2000). The complete atomic structure of the large ribosomal subunit at 2·4 Å resolution. *Science* **289**, 905–920.

Banham, J. E., Timmel, C. R., Abbott, R. J. M., Lea, S. M. & Jeschke, G. (2006). The characterization of weak protein–protein interactions: evidence from DEER for the trimerization of a von Willebrand Factor A domain in solution. *Angewandte Chemie International Edition* **45**, 1058–1061.

Becker, J. S. & Saxena, S. (2005). Double quantum coherence electron spin resonance on coupled Cu(II)–Cu(II) electron spins. *Chemical Physics Letters* **414**, 248–252.

Bennati, M., Lendzian, F., Schmittel, M. & Zipse, H. (2005a). Spectroscopic and theoretical approaches for studying radical reactions in class I ribonucleotide reductase. *Biological Chemistry* **386**, 1007–1022.

Bennati, M. & Prisner, T. F. (2005). New developments in high-field electron paramagnetic resonance with applications in structural biology. *Reports on Progress in Physics* **68**, 411–448.

Bennati, M., Robblee, J. H., Mugnaini, V., Stubbe, J., Freed, J. H. & Borbat, P. (2005b). EPR distance measurements support a model for long-range radical initiation in *E. coli* ribonucleotide reductase. *Journal of the American Chemical Society* **127**, 15014–15015.

Bennati, M., Weber, A., Antonic, J., Perlstein, D. L., Robblee, J. & Stubbe, J. (2003). Pulsed ELDOR spectroscopy measures the distance between the two tyrosyl radicals in the R2 subunit of the *E. coli* ribonucleotide reductase. *Journal of the American Chemical Society* **125**, 14988–14989.

Bennett, B., Antholine, W. E., D'souza, V. M., Chen, G., Ustinyuk, L. & Holz, R. C. (2002). Structurally distinct active sites in the copper(II)-substituted aminopeptidases from *Aeromonas proteolytica* and *Escherichia coli*. *Journal of the American Chemical Society* **124**, 13025–13034.

Berliner, L. J. (ed.) (1976). Spin labeling. Theory and applications. In *Molecular Biology*, New York: Academic Press.

Berliner, L. J. (ed.) (1998). Spin labeling. The next millennium. In *Biological Magnetic Resonance*, vol. 14. New York: Plenum Press.

Berliner, L. J., Eaton, S. S. & Eaton, G. R. (eds.) (2000). Distance measurements in biological systems by EPR. In *Biological Magnetic Resonance*, vol. 19. New York: Kluwer Academic/Plenum Publishers.

Berliner, L. J., Grunwald, J., Hankovszky, H. O. & Hideg, K. (1982). A novel reversible thiol-specific spin label: Papain active site labeling and inhibition. *Analytical Biochemistry* **119**, 450–455.

Berliner, L. J. & Reuben, J. (eds.) (1989). Spin labeling. Theory and applications. In *Biological Magnetic Resonance*, vol. 8. New York: Plenum Press.

Biglino, D., Schmidt, P. P., Reijerse, R. J. & Lubitz, W. (2006). PELDOR study on the tyrosyl radicals in the R2 protein of mouse ribonucleotide reductase. *Physical Chemistry Chemical Physics* **8**, 58–62.

Bittl, R. & Kawamori, A. (2005). Configuration of electron transfer components studied by EPR spectroscopy. In *Photosystem II The Light-Driven Water: Plastochinone Oxidoreductase*, vol. 22. *Advances in Photosynthesis and Respiration* (eds. T. J. Wydrzynski & K. Satoh), pp. 389–402. Dordrecht: Springer.

Bittl, R. & Kothe, G. (1991). Transient EPR of radical pairs in photosynthetic reaction centers: prediction of quantum beats. *Chemical Physics Letters* **177**, 547–553.

Bittl, R. & Weber, S. (2005). Transient radical pairs studied by time-resolved EPR. *Biochimica et Biophysica Acta-Bioenergetics* **1797**, 117–126.

Bittl, R. & Zech, S. G. (1997). Pulsed EPR study of spin-coupled radical pairs in photosynthetic reaction centers: measurement of the distance between $P_{700}^{\bullet+}$ and $A_1^{\bullet-}$ in

photosystem I and between $P_{865}^{\bullet+}$ and in bacterial reaction centers. *Journal of Physical Chemistry* **101**, 1429–1436.

Bittl, R. & Zech, S. G. (2001). Pulsed EPR spectroscopy on short-lived intermediates in photosystem I. *Biochimica et Biophysica Acta-Bioenergetics* **1507**, 194–211.

Blankenship, R. E., McGuire, A. & Sauer, K. (1975). Chemically induced dynamic electron polarization in chloroplasts at room temperature. *Proceedings of the National Academy of Sciences USA* **72**, 4943–4947.

Bobst, A. M., Pauly, G. T., Keyes, R. S. & Bobst, E. V. (1988). Enzymatic sequence-specific spin labeling of a DNA fragment containing the recognition sequence of *Eco*RI endonuclease. *Federation of European Biochemical Societies Letters* **228**, 33–36.

Bock, C. H., Stehlik, D. & Thurnauer, M. C. (1988). Experimental evidence for the anisotropic nature of the transient EPR spectrum from photosystem I observed in cyanobacteria. *Israel Journal of Chemistry* **28**, 177–182.

Bode, B. E., Margraf, D., Plackmeyer, J., Dürner, G., Prisner, T. F. & Schiemann, O. (2007). Counting the monomers in nanometer-sized oligomers by pulsed electron-electron double resonance. *Journal of the American Chemical Society*, DOI: 10.1021/ja065787t.

Bonora, M., Becker, J. & Saxena, S. (2004). Suppression of electron spin-echo envelope modulation peaks in double quantum coherence electron spin resonance. *Journal of Magnetic Resonance* **170**, 278–283.

Bonvin, A. M. J. J., Boelens, R. & Kaptein, R. (2005). NMR analysis of protein interactions. *Current Opinion in Chemical Biology* **9**, 783–790.

Borbat, P. P., Costa-Filho, A. J., Earle, K. A., Moscicki, J. K. & Freed, J. H. (2001). Electron spin resonance in studies of membranes and proteins. *Science* **291**, 266–269.

Borbat, P. P., Davis, J. H., Butcher, S. E. & Freed, J. H. (2004). Measurement of large distances in biomolecules using double-quantum filtered refocused electron spin-echoes. *Journal of the American Chemical Society* **126**, 7746–7747.

Borbat, P. P. & Freed, J. H. (1999). Multiple-quantum ESR and distance measurements. *Chemical Physics Letters* **313**, 145–154.

Borbat, P. P. & Freed, J. H. (2000). Double-quantum ESR and distance measurements. In *Distance Measurements in Biological Systems by EPR*, vol. 19 (eds. L. J. Berliner, S. S. Eaton & G. R. Eaton), pp. 383–459. New York: Kluwer Academic/Plenum Publishers.

Borbat, P. P., Mchaourab, H. S. & Freed, J. H. (2002). Protein structure determination using long-distance constraints from double-quantum coherence ESR: study of T4 lysozyme. *Journal of the American Chemical Society* **124**, 5304–5314.

Borbat, P. P., Ramlall, T. F., Freed, J. H. & Eliezer, D. (2006). Inter-helix distances in lysophospholipid micelle-bound α-synuclein from pulsed ESR measurements. *Journal of the American Chemical Society* **128**, 10004–10005.

Borovykh, I. V., Ceola, S., Gajula, P., Gast, P., Steinhoff, H.-J. & Huber, M. (2006). Distance between a native cofactor and a spin label in the reaction center of *Rhodobacter sphaeroides* by a two-frequency pulsed electron paramagnetic resonance method and molecular dynamics simulations. *Journal of Magnetic Resonance* **180**, 178–185.

Borovykh, I. V., Kulik, L. V., Gast, P. & Dzuba, S. A. (2003). Conformation transition in the protein of a photosynthetic reaction center observed at the nanometer range of distances at cryogenic temperatures. *Chemical Physics* **294**, 433–438.

Bowman, M. K., Becker, D., Sevilla, M. D. & Zimbrick, J. D. (2005). Track structure in DNA irradiated with heavy ions. *Radiation Research* **163**, 447–454.

Bowman, M. K., Maryasov, A. G., Kim, N. & DeRose, V. J. (2004). Visualization of distance distribution from pulsed double electron–electron resonance data. *Applied Magnetic Resonance* **26**, 23–39.

Brown, L. J., Sale, K., Hills, R., Rouviere, C., Song, L., Zhang, X. & Fajer, P. (2002). Structure of the inhibitory region of troponin by site directed spin labeling electron paramagnetic resonance. *Proceedings of the National Academy of Sciences USA* **99**, 12765–12770.

Brudvig, G. W., Blair, D. F. & Chan, S. I. (1984). Electron spin relaxation of Cu_A and cytochrome *a* in cytochrome *c* oxidase. *Journal of Biological Chemistry* **259**, 11001–11009.

Cai, Q., Kusnetzow, A. K., Hubbell, W. L., Haworth, I. S., Gacho, G. P. C., Eps, N. V., Hideg, K., Chambers, E. J. & Qin, P. Z. (2006). Site-directed spin labeling measurements of nanometer distances in nucleic acids using a sequence-independet nitroxide probe. *Nucleic Acids Research* **34**, 4722–4730.

Calle, C., Sreekanth, A., Fedin, M. V., Forrer, J., Garcia-Rubio, I., Gromov, I. A., Hinderberger, D., Kasumaj, B., Léger, P., Mancosu, B., Mitrikas, G., Santangelo, M. G., Stoll, S., Schweiger, A., Tschaggelar, R. & Harmer, J. (2006). Pulse EPR methods for studying chemical and biological samples containing transition metals. *Helvetica Chimica Acta* **89**, 2495–2521.

Caron, M. & Dugas, H. (1976). Specific spin-labeling of transfer ribonucleic acid molecules. *Nucleic Acids Research* **3**, 19–34.

Cekan, P. & Sigurdsson, S. T. (2005). Spin labeled nucleic acids for EPR spectroscopic study of DNA and RNA structure and function. *Collection Symposium Series* **7**, 225–228.

Chiang, Y.-W., Borbat, P. P. & Freed, J. H. (2005a). The determination of pair distance distributions by pulsed EPR using Tikhonov regularization. *Journal of Magnetic Resonance* **172**, 279–295.

CHIANG, Y.-W., BORBAT, P. P. & FREED, J. H. (2005b). Maximum entropy: a complement to Tikhonov regularization for determination of pair distance distributions by pulsed EPR. *Journal of Magnetic Resonance* **177**, 184–196.

CODD, R., ASTASHKIN, A. V., PACHECO, A., RAITSIMRING, A. M. & ENEMARK, J. H. (2002). Pulsed ELDOR spectroscopy of the Mo(V)/Fe(III) state of sulfite oxidase prepared by one-electron reduction with Ti(III) citrate. *Journal of Biological Inorganic Chemistry* **7**, 338–350.

CRAMER, P., BUSHNELL, D. A. & KORNBERG, R. D. (2001). Structural basis of transcription: RNA polymerase II at 2·8 Å resolution. *Science* **292**, 1863–1876.

DARIAN, E. & GANNETT, P. M. (2005). Application of molecular dynamics simulations to spin-labeled oligonucleotides. *Journal of Biomolecular Structure & Dynamics* **22**, 579–593.

DEISENHOFER, J., MIKI, K., HUBER, R. & MICHEL, H. (1986). Structure of the protein subunits in the photosynthetic reaction center of *Rhodopseudomonas viridis* at 3 Å resolution. *Nature* **318**, 618–624.

DELIGIANNAKIS, Y. & RUTHERFORD, A. W. (1996). Spin-lattice relaxation of the pheophytin, $Pheo^{-}$, radical of photosystem II. *Biochemistry* **35**, 11239–11246.

DENYSENKOV, V. P., PRISNER, T. F., STUBBE, J. & BENNATI, M. (2005). High-frequency 180 GHz PELDOR. *Applied Magnetic Resonance* **29**, 375–384.

DENYSENKOV, V. P., PRISNER, T. F., STUBBE, J. & BENNATI, M. (2006). High-field pulsed electron–electron double resonance spectroscopy to determine the orientation of the tyrosyl radicals in ribonucleotide reductase. *Proceedings of the National Academy of Sciences USA* **103**, 13386–13390.

DONALDSON, L. W., SKRYNNIKOV, N. R., CHOY, W.-Y., MUHANDIRAM, D. R., SARKAR, B., FORMAN-KAY, J. D. & KAY, L. E. (2001). Structural characterization of proteins with an attached ATCUN motif by paramagnetic relaxation enhancement NMR spectroscopy. *Journal of the American Chemical Society* **123**, 9843–9847.

DZIKOVSKI, B. G., BORBAT, P. P. & FREED, J. H. (2004). Spin-labeled Gramicidin A: channel formation and dissociation. *Biophysical Journal* **87**, 3504–3517.

DZUBA, S. A., GAST, P. & HOFF, A. J. (1995). ESEEM study of spin–spin interactions in spin-polarized $P^{+}Q_{A}^{-}$ pairs in the photosynthetic purple bacterium *Rhodobacter sphaeroides* R26. *Chemical Physics Letters* **236**, 595–602.

DZUBA, S. A., GAST, P. & HOFF, A. J. (1997). Probing the energy landscape of bacterial photosynthetic reaction centers at cryogenic temperatures by ESEEM of spin-polarized $D^{+}Q_{A}^{-}$ radical pairs. *Chemical Physics Letters* **268**, 273–279.

DZUBA, S. A. & HOFF, A. J. (2000). Photo-induced radical pairs investigated using out-of-phase Electron Spin echo. In *Distance Measurements in Biological Systems by EPR, Biological Magnetic Resonance*, vol. 19 (eds. L. J. Berliner, S. S. Eaton & G. R. Eaton), pp. 569–596. New York: Kluwer Academic/Plenum Publishers.

EATON, S. S. & EATON, G. R. (2002). Electron paramagnetic resonance techniques for measuring distances in proteins. *Structures and Mechanisms: from ashes to enzymes. ACS Symposium Series* **827**, 321–339.

EATON, S. S. & EATON, G. R. (2004). Measurements of interspin distances by EPR. *Specialist Periodical Reports on Electron Spin Resonance* **19**, 318–337.

EDWARDS, T. E., OKONOGI, T. M., ROBINSON, B. H. & SIGURDSSON, S. T. (2001). Site-specific incorporation of nitroxide spin-labels into internal sites of the TAR RNA; Structure-dependent dynamics of RNA by EPR spectroscopy. *Journal of the American Chemical Society* **123**, 1527–1528.

ELSÄSSER, C., BRECHT, M. & BITTL, R. (2002). Pulsed electron–electron double resonance on multinuclear metal clusters: assignment of spin projection factors based on the dipolar interaction. *Journal of the American Chemical Society* **124**, 12606–12611.

ELSÄSSER, C., BRECHT, M. & BITTL, R. (2005). Treatment of spin-coupled metal-centres in pulsed electron–electron double-resonance experiments. *Biochemical Society Transactions* **33**, 15–19.

ERNST, R. R. (1992). Nuclear magnetic resonance Fourier transform spectroscopy. *Angewandte Chemie International Edition* **31**, 805–823.

ERNST, R. R., BODENHAUSEN, G. & WOKAUN, A. (1990). *Principles of Nuclear Magnetic Resonance in One and Two Dimensions*. Oxford: Clarendon Press.

EST, A. V. D., BITTL, R., ABRESCH, E. C., LUBITZ, W. & STEHLIK, D. (1993). Transient EPR spectroscopy of perdeuterated Zn-substituted reaction centers of *Rhodobacter sphaeroides* R-26. *Chemical Physics Letters* **212**, 561–568.

EST, A. V. D., PRISNER, T. F., BITTL, R., FROMME, P., LUBITZ, W., MÖBIUS, K. & STEHLIK, D. (1997). Time resolved multi-frequency EPR of the state $P_{700}^{+\bullet}$ $A_{1}^{-\bullet}$ in Photosystem I of *Synechoccus elongatus* and a comparison with P_{865}^{+} Q_{A}^{-} in reaction centres of *Rhodobacter sphaeroides* R-26. *Journal of Physical Chemistry B* **101**, 1437.

FAJER, P. G. (2005). Site directed spin labeling and pulsed dipolar electron paramagnetic resonance (double electron–electron resonance) of force activation in muscle. *Journal of Physics* **17**, S1459–S1469.

FARRENS, D., ALTENBACH, C., YANG, K., HUBBELL, W. L. & KHORANA, H. G. (1996). Requirement of rigid-body motion of transmembrane helices for light activation of Rhodopsin. *Science* **274**, 768–770.

FREED, J. H. (2000). New technologies in electron spin resonance. *Annual Reviews of Physical Chemistry* **51**, 655–689.

FRITSCHER, J., ARTIN, E., WNUK, S., BAR, G., ROBBLEE, J. H., KACPRZAK, S., KAUPP, M., GRIFFIN, R. G., BENNATI, M. & STUBBE, J. (2005). Structure of the nitrogen-centered radical formed during inactivation of *E. coli*

ribonucleotide reductase by 2′-azido-2′-deoxyuridine-5′-diphosphate: trapping of the 3′-ketonucleotide. *Journal of the American Chemical Society* **127**, 7729–7738.

Gannett, P. M., Darian, E., Powell, J., Johnson, E. M. I., Mundoma, C., Greenbaum, N. L., Ramsey, C. M., Dalal, N. S. & Budil, D. E. (2002). Probing triplex formation by EPR spectroscopy using a newly synthesized spin label for oligonucleotides. *Nucleic Acids Research* **30**, 5328–5337.

Gnatt, A. L., Cramer, P., Fu, J., Bushnell, D. A. & Kornberg, R. D. (2001). Structural basis of transcription: an RNA polymerase II elongation complex at 3·3 Å resolution. *Science* **292**, 1876–1882.

Godt, A., Franzen, C., Veit, S., Enkelmann, V., Pannier, M. & Jeschke, G. (2000). EPR probes with well-defined, long distances between two or three unpaired electrons. *Journal of Organic Chemistry* **65**, 7575–7582.

Godt, A., Schulte, M., Zimmermann, H. & Jeschke, G. (2006). How flexible are poly(paraphenyleneethynylene)s? *Angewandte Chemie International Edition* **45**, 7722–7726.

Golombek, A. P. & Hendrich, M. P. (2003). Quantitative analysis of dinuclear manganese(II) EPR spectra. *Journal of Magnetic Resonance* **165**, 33–48.

Goodman, G., John, S. & Leigh, J. (1985). Distance between the visible copper and cytochrome *a* in bovine heart cytochrome oxidase. *Biochemistry* **24**, 2310–2317.

Gordeliy, V. I., Labahn, J., Moukhametzianov, R., Efremov, R., Granzin, J., Schlesinger, R., Büldt, G., Savopol, T., Scheidig, A. J., Klare, J. P. & Engelhard, M. (2002). Molecular basis of transmembrane signalling by sensory rhodopsin II-transducer complex. *Nature* **419**, 484–487.

Gullion, T. & Schaefer, J. (1989). Rotational-echo double-resonance NMR. *Journal of Magnetic Resonance* **81**, 196–200.

Gullion, T. & Vega, A. J. (2005). Measuring heteronuclear dipolar couplings for $I=1/2$, $S>1/2$ spin pairs by REDOR and REAPDOR NMR. *Progress in Nuclear Magnetic Resonance Spectroscopy* **47**, 123–136.

Hanson, P., Millhauser, G. L., Formaggio, F., Crisma, M. & Toniolo, C. (1996). ESR characterization of hexameric, helical peptides using double TOAC spin labeling. *Journal of the American Chemical Society* **118**, 7618–7625.

Hara, H., Dzuba, S. A., Kawamori, A., Akabori, K., Tomo, T., Satoh, K., Iwaki, M. & Itoh, S. (1997). The distance between P680 and Q_A in Photosystem II determined by ESEEM spectroscopy. *Biochimica et Biophysica Acta* **1322**, 77–85.

Hara, H., Horiuche, T., Saneyoshi, M. & Nishimura, S. (1970). 4-Thiouridine-specific spin-labeling. *Biochemical and Biophysical Research Communications* **38**, 305–311.

Hara, H., Kawamori, A., Astashkin, A. V. & Ono, T.-A. (1996). The distances from tyrosine D to redox-active components on the donor side of photosystem II determined by pulsed electron-electron double resonance. *Biochimica et Biophysica Acta* **1276**, 140–146.

Hertel, M. M., Denysenkov, V. P., Bennati, M. & Prisner, T. F. (2005). Pulsed 180-GHz EPR/ENDOR/PELDOR spectroscopy. *Magnetic Resonance in Chemistry* **43**, S248–S255.

Hilger, D., Jung, H., Padan, E., Wegener, C., Vogel, K.-P., Steinhoff, H.-J. & Jeschke, G. (2005). Assessing oligomerization of membrane proteins by four-pulse DEER: pH-dependent dimerization of NhaA Na^+/H^+ antiporter of *E. coli*. *Biophysical Journal* **89**, 1328–1338.

Hirsh, D. J., Beck, W. F., Innes, J. B. & Brudvig, G. W. (1992). Using saturation-recovery EPR to measure distances in proteins: applications to photosystem II. *Biochemistry* **31**, 532–541.

Hoff, A. J. (ed.) (1989). Advanced EPR. Applications in Biology and Biochemistry. Amsterdam: Elsevier.

Hoff, A. J., Gast, P. & Romijn, J. C. (1977). Time-resolved ESR and chemically induced dynamic electron polarization of the primary reaction in a reaction center of *Rhodopseudomonas sphaeroides* wild type at low temperatures. *Federation of European Biochemical Societies Letters* **73**, 185–190.

Högbom, M., Galander, M., Andersson, M., Kolberg, M., Hofbauer, W., Lassmann, G., Nordlund, P. & Lendzian, F. (2003). Displacement of the tyrosyl radical cofactor in ribonucleotide reductase obtained by single-crystal high-field EPR and 1·4 Å X-ray data. *Proceedings of the National Academy of Sciences USA* **100**, 3209–3214.

Hore, P. J., Hunter, D. A., McKie, C. D. & Hoff, A. J. (1987). Electron paramagnetic resonance of spin-correlated radical pairs in photosynthetic reactions. *Chemical Physics Letters* **137**, 459–500.

Hubbell, W. L., Cafiso, D. S. & Altenbach, C. (2000). Identifying conformational changes with site-directed spin labeling. *Nature Structural Biology* **7**, 735–739.

Hubbell, W. L., Gross, A., Langen, R. & Lietzow, M. A. (1998). Recent advances in site-directed spin labeling of proteins. *Current Opinion in Structural Biology* **8**, 649–656.

Hung, S.-C., Grant, C. V., Peloquin, J. M., Waldeck, A. R., Britt, R. D. & Chan, S. I. (2000). Electron spin-lattice relaxation measurement of the 3Fe–4S (S-3) cluster in succinate:ubiquinone reductase from *Paracoccus denitrificans*. A detailed analysis based on a dipole–dipole interaction model. *Journal of Physical Chemistry B* **104**, 4402–4412.

Hustedt, E. J. & Beth, A. H. (1999). Nitroxide spin–spin interactions: applications to protein structure and dynamics. *Annual Review of Biophysics and Biomolecular Structure* **28**, 129–153.

Hustedt, E. J. & Beth, A. H. (2000). Structural information from CW-EPR spectra of dipolar coupled nitroxide spin labels. In *Distance Measurements in Biological Systems by EPR*, vol. 19 (eds. L. J. Berliner, S. S. Eaton

& G. R. Eaton), pp. 155–184. New York: Kluwer Academic/Plenum Publishers.

Hustedt, E. J., Smirnov, A. I., Laub, C. F., Cobb, C. E. & Beth, A. H. (1997). Molecular distances from dipolar coupled spin labels: the global analysis of multifrequency continuous wave electron paramagnetic resonance data. *Biophysical Journal* **74**, 1861–1877.

Hustedt, E. J., Stein, R. A., Sethaphong, L., Brandon, S., Zhou, Z. & DeSensi, S. C. (2006). Dipolar coupling between nitroxide spin labels: the development and application of a tether-in-a-cone model. *Biophysical Journal* **90**, 340–345.

Iwahara, J. & Clore, G. M. (2006). Detecting transient intermediates in macromolecular binding by paramagnetic NMR. *Nature* **440**, 1227–1230.

Jeschke, G. (2002). Determination of the nanostructure of polymer materials by electron paramagnetic resonance spectroscopy. *Macromolecular Rapid Communications* **23**, 227–246.

Jeschke, G., Bender, A., Paulsen, H., Zimmermann, H. & Godt, A. (2004a). Sensivity enhancement in pulse EPR distance measurements. *Journal of Magnetic Resonance* **169**, 1–12.

Jeschke, G., Bender, A., Schweikardt, T., Panek, G., Decker, H. & Paulsen, H. (2005). Localization of the N-terminal domain in light-harvesting chlorophyll *a/b* protein by EPR measurements. *Journal of Biological Chemistry* **280**, 18623–18630.

Jeschke, G., Koch, A., Jonas, U. & Godt, A. (2002). Direct conversion of EPR dipolar time evolution data to distance Distributions. *Journal of Magnetic Resonance* **155**, 72–82.

Jeschke, G., Panek, G., Godt, A., Bender, A. & Paulsen, H. (2004b). Data analysis procedures for pulse ELDOR measurements of broad distance distributions. *Applied Magnetic Resonance* **26**, 223–244.

Jeschke, G., Pannier, P., Godt, A. & Spiess, H. W. (2000). Dipolar spectroscopy and spin alignment in electron paramagnetic resonance. *Chemical Physics Letters* **331**, 243–252.

Jeschke, G. & Schlick, S. (2006). Spatial distribution of stabilizer-derived nitroxide radicals during thermal degradation of poly(acrylonitrile-butadiene-styrene) copolymers: a unified picture from pulsed ELDOR and ESR imaging. *Physical Chemistry Chemical Physics* **8**, 4095–4103.

Jeschke, G., Wegener, C., Nietschke, M., Jung, H. & Steinhoff, H.-J. (2004c). Interresidual distance determination by four-pulse double electron–electron resonance in an integral membrane protein: the Na^+/proline transporter PutP of *Escherichia coli*. *Biophysical Journal* **86**, 2551–2557.

Jeschke, G., Zimmermann, H. & Godt, A. (2006). Isotope selection in distance measurements between nitroxides. *Journal of Magnetic Resonance* **180**, 137–146.

Jun, S., Becker, J. S., Yonkunas, M., Coalson, R. & Saxena, S. (2006). Unfolding of alanine-based peptides using electron spin resonance distance measurements. *Biochemistry* **45**, 11666–11673.

Kahn, O. (1993). *Molecular Magnetism*. New York: Wiley-VCH.

Käss, H., MacMillan, F., Ludwig, B. & Prisner, T. F. (2000). Investigation of the Mn binding site in cytochrome *c* oxidase from *Paracoccus denitrificans* by high-frequency EPR. *Journal of Physical Chemistry B* **104**, 5362–5371.

Käss, H., Stürzel, M., Ludwig, B., Dinse, K. P. & Prisner, T. F. (1998). Investigation of a Mn binding site in cytochrome *c* oxidase by high-frequency EPR. *Proceedings of the 28th Congress AMPERE on Magnetic Resonance and Related Phenomena*, 877.

Kawamori, A., Katsuta, N. & Hara, H. (2003). Structural analysis of three-spin systems of photosystem II by PELDOR. *Applied Magnetic Resonance* **23**, 557–569.

Kawamori, A., Katsuta, N., Mino, H., Ishii, A., Minagawa, J. & Ono, T.-A. (2002). Positions of Q_A and Chl_Z relative to tyrosine Y_Z and Y_D in photosystem II studied by pulsed EPR. *Journal of Biological Physics* **28**, 413–426.

Kawamori, A., Ono, T.-A., Ishii, A., Nakazawa, S., Hara, H., Tomo, T., Minagawa, J., Bittl, R. & Dzuba, S. A. (2005). The functional site of chlorophylls in D1 and D2 subunits of photosystem II identified by pulsed EPR. *Photosynthesis Research* **84**, 187–192.

Kay, C. W. M., Elsässer, C., Bittl, R., Farrell, S. R. & Thorpe, C. (2006). Determination of the distance between the two neutral flavin radicals in augmenter of liver regeneration by Pulsed ELDOR. *Journal of the American Chemical Society* **128**, 76–77.

Keyes, R. S. & Bobst, A. M. (1998). Spin-labeled nucleic acids. In *Spin Labeling. The Next Millennium*, vol. 14 (ed. L. J. Berliner), pp. 283–338. New York: Plenum Press.

Khangulov, S. V., Pessiki, P. J., Barynin, V. V., Ash, D. E. & Dismukes, G. C. (1995). Determination of the metal ion separation and energies of the three lowest electronic states of dimanganese(II,II) complexes and enzymes: catalase and liver arginase. *Biochemistry* **34**, 2015–2025.

Kim, N.-K., Murali, A. & DeRose, V. J. (2004). A distance ruler for RNA using EPR and site-directed spin labeling. *Chemistry & Biology* **11**, 939–948.

Klare, J. P., Gordeliy, V. I., Labahn, J., Büldt, G., Steinhoff, H.-J. & Engelhard, M. (2004). The archaeal sensory rhodopsin II/transducer complex: a model for transmembrane signal transfer. *Federation of European Biochemical Societies Letters* **564**, 219–224.

Kodera, Y., Dzuba, S. A., Hara, H. & Kawamori, A. (1994). Distances from tyrosine D^+ to the manganese cluster and the acceptor iron in Photosystem II as determined by selective hole burning in EPR spectra. *Biochimica et Biophysica Acta* **1186**, 91–99.

Kokorin, A. I., Zamarayev, K. I., Grigoryan, G. L., Ivanov, V. P. & Rozantsev, E. G. (1972). Measurements of the distance between the paramagnetic centers in solid solutions of nitroxide radicals, biradicals, and spin-labeled proteins. *Biofizika* **17**, 34–41.

Kolberg, M., Strand, K. R., Graff, P. & Andersson, K. K. (2004). Structure, function, and mechanism of ribonucleotide reductase. *Biochimica et Biophysica Acta* **1699**, 1–34.

Kothe, G., Weber, S., Bittl, R., Ohmes, E., Thurnauer, M. C. & Norris, J. R. (1991). Transient EPR of light-induced radical pairs in plant photosystem I: observation of quantum beats. *Chemical Physics Letters* **186**, 474–479.

Kothe, G., Weber, S., Ohmes, E., Thurnauer, M. C. & Norris, J. R. (1994). High time resolution electron paramagnetic resonance of light-induced radical pairs in photosynthetic bacterial reaction centers: observation of quantum beats. *Journal of the American Chemical Society* **116**, 7729–7734.

Kulik, L. V., Borovykh, I. V., Gast, P. & Dzuba, S. A. (2003). Selective excitation in pulsed EPR of a spin-correlated triplet-radical pair. *Journal of Magnetic Resonance* **162**, 423–428.

Kulik, L. V., Dzuba, S. A., Grigoryev, I. A. & Tsvetkov, Y. D. (2001). Electron dipole–dipole interaction in ESEEM of nitroxide biradicals. *Chemical Physics Letters* **343**, 315–324.

Kulik, L. V., Pachenko, S. V. & Dzuba, S. A. (2002). 130 GHz ESEEM induced by electron–electron interaction in biradicals. *Journal of Magnetic Resonance* **159**, 237–241.

Kulikov, A. V. & Likhtenstein, G. I. (1977). The use of spin relaxation phenomena in the investigation of the structure of model and biological systems by the method of spin labels. *Advances in Molecular Relaxation and Interaction Processes* **10**, 47–79.

Kuroiwa, S., Tonaka, M., Kawamori, A. & Akabori, K. (2000). The position of cytochrome b_{559} relative to Q_A in photosystem II studied by electron–electron double resonance (ELDOR). *Biochimica et Biophysica Acta* **1460**, 330–337.

Kurshev, V. V., Raitsimring, A. M. & Tsvetkov, Y. D. (1988). Selection of dipolar interaction by the '2+1' pulse traLn ESE. *Institute of Chemical Kinetics and Combustion*, 441–455.

Lakowicz, J. R. (2006). *Principles of Fluorescence Spectroscopy*, 3rd edn. New York: Springer.

Lakshmi, K. V. & Brudvig, G. W. (2000). Electron paramagnetic resonance distance measurements in photosynthetic reaction centers. In *Distance Measurements in Biological Systems by EPR, Biological Magnetic Resonance*, vol. 19 (eds. L. J. Berliner, S. S. Eaton & G. R. Eaton), pp. 513–567. New York: Kluwer Academic/Plenum Publishers.

Lakshmi, K. V. & Brudvig, G. W. (2001). Pulsed electron paramagnetic resonance methods for macromolecular structure determination. *Biophysical Methods* **11**, 523–531.

Lakshmi, K. V., Poluektov, O. G., Reifler, M. J., Wagner, A. M., Thurnauer, M. C. & Brudvig, G. W. (2003). Pulsed high-frequency EPR study on the location of carotenoid and chlorophyll cation radicals in photosystem II. *Journal of the American Chemical Society* **125**, 5005–5014.

Langen, R., Oh, K.-J., Cascio, D. & Hubbell, W. L. (2000). Crystal structures of spin labeled T4 Lysozyme mutants: implications for the interpretation of EPR spectra in terms of structure. *Biochemistry* **39**, 8396–8405.

Larsen, R. G. & Sigel, D. J. (1993). Double electron-electron resonance spin-echo modulation: spectroscopic measurement of electron spin pair separations in orientationally disordered solids. *Journal of Chemical Physics* **98**, 5134–5146.

Liang, Z. L., Freed, J. H., Keyes, R. S. & Bobst, A. M. (2000). An electron spin resonance study of DNA dynamics using the slowly relaxing local structure model. *Journal of Physical Chemistry B* **104**, 5372–5381.

Likhtenshtein, G. I. (1993). *Biophysical Labeling Methods in Molecular Biology*. Cambridge: Cambridge University Press.

Link, G., Berthold, T., Bechtold, M., Weidner, J.-U., Ohmes, E., Tang, J., Poluektov, O., Utschig, L., Schlesselman, S. L., Thurnauer, M. C. & Kothe, G. (2001). Structure of the P_{700}^{+} A_1^{-} radical pair intermediate in photosystem I by high time resolution multi-frequency electron paramagnetic resonance: analysis of quantum beat oscillations. *Journal of the American Chemical Society* **123**, 4211–4222.

Liu, Y.-S., Sompornpisut, P. & Perozo, E. (2001). Structure of the KcsA channel intracellular gate in the open state. *Nature Structural Biology* **8**, 883–887.

Loll, B., Kern, J., Saenger, W., Zouni, A. & Biesiadka, J. (2005). Towards complete cofactor arrangement in the 3·0 Å resolution structure of photosystem II. *Nature* **438**, 1040–1044.

Lubitz, W. (2004). EPR in Photosynthesis. In *Electron Paramagnetic Resonance*, vol. 19 (ed. D. M. Murphy), pp. 174–242. London: Royal Society of Chemistry.

Lubitz, W. & Feher, G. (1999). The primary and secondary acceptors in bacterial photosynthesis III. Characterization of the quinone radicals $Q_A^{-\bullet}$ and $Q_B^{-\bullet}$ by EPR and ENDOR. *Applied Magnetic Resonance* **17**, 1–48.

Lubitz, W., Lendzian, F. & Bittl, R. (2002). Radicals, radical pairs and triplet states in photosynthesis. *Accounts of Chemical Research* **35**, 313–320.

Luoma, G. A., Herring, F. G. & Marshall, A. G. (1982). Flexibility of end-labeled polymers from electron spin resonance line-shape analysis: 3′ terminus of transfer ribonucleic acid and 5S ribonucleic acid. *Biochemistry* **21**, 6591–6598.

Lyubenova, S., Siddiqui, M. K., Penning de Vries, M. J. M., Ludwig, B. & Prisner, T. F. (2007). Protein-Protein Interactions Studied by EPR Relaxation Measurements: Cytochrome *c* and Cytochrome *c* Oxidase. *Journal of Physical Chemistry B* **111**, 3839–3846.

MacArthur, R. & Brudvig, G. W. (2004). Location of EPR-active spins buried in proteins from the simulation of the spin-lattice relaxation enhancement caused by Dy(III) complexes. *Journal of Physical Chemistry B* **108**, 9390–9396.

Macosko, J. C., Pio, M. S., Tinoco, I. & Shin, Y.-K. (1999). A novel 5′ displacement spin-labeling technique for electron paramagnetic resonance spectroscopy of RNA. *RNA* **5**, 1158–1166.

Mamedov, F., Smith, P. J., Styring, S. & Pace, R. J. (2004). Relaxation behaviour of the tyrosine Y_D radical in photosystem II: evidence for strong dipolar interaction with paramagnetic centers in the S_1 and S_2 states. *Physical Chemistry Chemical Physics* **6**, 4890–4896.

Marchetto, R., Schreier, S. & Nakaie, C. R. (1993). A novel spin-labeled amino acid derivative for use in peptide synthesis: (9-Fluorenylmethyloxycarbonyl)-2,2,6,6-tetramethylpiperidine-*N*-oxyl-4-amino-4-carboxylic Acid. *Journal of the American Chemical Society* **115**, 11042–11043.

Marsh, D. & Horvath, L. I. (1989). Spin label studies of the structure and dynamics of lipids and proteins in membranes. In *Advanced EPR. Applications in Biology and Biochemistry* (ed. A. J. Hoff), pp. 707–752. Amsterdam: Elsevier.

Martin, R. E., Pannier, M., Diederich, F., Gramlich, V., Hubrich, M. & Spiess, H. W. (1998). Determination of end-to-end distances in a series of TEMPO diradicals of up to 2·8 nm length with a new four-pulse double electron–electron resonance experiment. *Angewandte Chemie International Edition* **37**, 2834–2837.

McIntosh, A. R., Caron, M. & Dugas, H. (1973). A specific spin labeling of the anticodon of *E. coli* $tRNA^{Glu}$. *Biochemical and Biophysical Research Communications* **55**, 1356–1362.

McNulty, J. C. & Millhauser, G. L. (2000). TOAC. The rigid nitroxide side chain. In *Distance Measurements in Biological Systems by EPR*, vol. 19 (eds L. J. Berliner, S. S. Eaton & G. R. Eaton), pp. 277–307. New York: Kluwer Academic/Plenum Publishers.

Mehring, M. & Weberruß, V. A. (2001). *Object-Oriented Magnetic Resonance*. San Diego: Academic Press.

Miller, T. R., Alley, S. C., Reese, A. W., Solomon, M. S., MacCallister, W. V., Mailer, C., Robinson, B. H. & Hopkins, P. B. (1995). A probe for sequence-dependent nucleic acid dynamics. *Journal of the American Chemical Society* **117**, 9377–9378.

Milov, A. D., Erilov, D. A., Salnikov, E. S., Tsvetkov, Y. D., Formaggio, F., Toniolo, C. & Raap, J. (2005). Structure and spatial distribution of the spin-labeled lipopeptide trichogin GA IV in a phospholipid membrane studied by pulsed electron–electron double resonance (PELDOR). *Physical Chemistry Chemical Physics* **7**, 1794–1799.

Milov, A. D., Maryasov, A. G. & Tsvetkov, Y. D. (1998). Pulsed electron double resonance (PELDOR) and its applications in free-radicals research. *Applied Magnetic Resonance* **15**, 107–143.

Milov, A. D., Maryasov, A. G., Tsvetkov, Y. D. & Raap, J. (1999). Pulsed ELDOR in spin-labeled polypeptides. *Chemical Physics Letters* **303**, 135–143.

Milov, A. D., Ponomarev, A. B. & Tsvetkov, Y. D. (1984). Electron–electron double resonance in electron spin echo: model biradical systems and the sensitized photolysis of decalin. *Chemical Physics Letters* **110**, 67–72.

Milov, A. D., Salikhov, K. M. & Shchirov, M. D. (1981). Application of the double resonance method to electron spin echo in a study of the spatial distribution of paramagnetic centers in solids. *Sovietscaya Physics Solid Stated* **23**, 565–569.

Milov, A. D., Samoilova, R. I., Tsvetkov, Y. D., Peggion, C., Formaggio, F., Toniolo, C. & Raap, J. (2006). Aggregation on spin-labeled alamethicin in low-polarity solutions as studied by PELDOR spectroscopy. *Physical Chemistry* **406**, 21–25.

Milov, A. D., Tsvetkov, Y. D., Formaggio, F., Crisma, M., Toniolo, C. & Raap, J. (2000). Self-assembling properties of membrane-modifying peptides studied by PELDOR and CW-ESR spectroscopies. *Journal of the American Chemical Society* **122**, 3843–3848.

Milov, A. D., Tsvetkov, Y. D., Formaggio, F., Crisma, M., Toniolo, C. & Raap, J. (2001). The secondary structure of a membrane-modifying peptide in a supramolecular assembly studied by PELDOR and CW-ESR spectroscopies. *Journal of the American Chemical Society* **123**, 3784–3789.

Milov, A. D., Tsvetkov, Y. D., Formaggio, F., Oancea, S., Toniolo, C. & Raap, J. (2003). Aggregation of spin labeled trichogin GA IV dimers: distance distributions between spin labels in frozen solutions by PELDOR data. *Journal of Physical Chemistry* **107**, 13719–13727.

Milov, A. D., Tsvetkov, Y. D., Formaggio, F., Oancea, S., Toniolo, C. & Raap, J. (2004). Solvent effect on the distance distribution between spin labels in aggregated spin labeled trichogin GA IV dimer peptides as studied by pulsed electron–electron double resonance. *Physical Chemistry Chemical Physics* **6**, 3596–3603.

Milov, A. D., Tsvetkov, Y. D., Gorbunova, E. Y., Mustaeva, L. G., Ovchinnikova, T. V. & Raap, J. (2002). Self-aggregation properties of spin-labeled zervamicin IIA as studied by PELDOR spectroscopy. *Biopolymers* **64**, 328–336.

Mims, W. B. (1972). Electron spin echos. In *Electron Paramagnetic Resonance* (ed. S. Geschwind), pp. 263–351. New York: Plenum.

Mino, H., Kawamori, A. & Ono, T.-A. (2000). Pulsed EPR studies of doublet signal and singlet-like signal in

oriented Ca^{2+}-depleted PS II membranes: location of the doublet signal center in PS II. *Biochemistry* **39**, 11034–11040.

Möbius, K., Savitsky, A., Schnegg, A., Plato, M. & Fuchs, M. (2005). High-field EPR spectroscopy applied to biological systems: characterization of molecular switches for electron and ion transfer. *Physical Chemistry Chemical Physics* **7**, 19–42.

Nagahara, S., Murakami, A. & Makino, K. (1992). Spin-labeled oligonucleotides site specifically labeled at the internucleotide linkage. Separation of stereoisomeric probes and EPR spectroscopical detection of hybrid formation in solution. *Nucleosides and Nucleotides* **11**, 889–901.

Narr, E., Godt, A. & Jeschke, G. (2002). Selective measurements of a nitroxide–nitroxide separation of 5 nm and a nitroxide-copper separation of 2·5 nm in a terpyridine-based copper(II) complex by pulse EPR spectroscopy. *Angewandte Chemie International Edition* **41**, 3907–3910.

Nissen, P., Hansen, J., Ban, N., Moore, P. B. & Steitz, T. A. (2000). The structural basis of ribosome activity in peptide bond synthesis. *Science* **289**, 920–930.

Nordlund, P., Sjöberg, B.-M. & Eklund, H. (1990). Three-dimensional structure of the free radical protein of ribonucleotide reductase. *Nature* **345**, 593–598.

Okonogi, T. M., Alley, S. C., Reese, A. W., Hopkins, P. B. & Robinson, B. H. (2000). Sequence-dependent dynamics in duplex DNA. *Biophysical Journal* **78**, 2560–2571.

Ostermeier, C., Harrenga, A., Ermler, U. & Michel, H. (1997). Structure at 2·7 Å resolution of the *Paracoccus denitrificans* two-subunit cytochrome *c* oxidase complexed with an antibody F-V fragment. *Proceedings of the National Academy of Sciences USA* **94**, 10547–10553.

Páli, T., Finbow, M. E. & Marsh, D. (2006). A divalent-ion binding site on the 16-kDa proton channel from *Nephrops norvegicus* – revealed by EPR spectroscopy. *Biochimica et Biophysica Acta* **1758**, 206–212.

Pannier, M., Veit, S., Godt, A., Jeschke, G. & Spiess, H. W. (2000). Dead-time free measurement of dipole-dipole interactions between electron spins. *Journal of Magnetic Resonance* **142**, 331–340.

Park, S.-Y., Borbat, P. P., Gonzalez-Bonet, G., Bhatnagar, J., Pollard, A. M., Freed, J. H., Bilwes, A. M. & Crane, B. R. (2006). Reconstruction of the chemotaxis receptor-kinase assembly. *Nature Structural & Molecular Biology* **13**, 400–407.

Perozo, E. (2002). New structural perspectives on K^+ channel gating. *Structure* **10**, 1027–1029.

Perozo, E., Cortes, D. M. & Cuello, L. G. (1999). Structural rearrangements underlying K^+-channel activation gating. *Science* **285**, 73–78.

Perozo, E., Cortes, D. M., Sompornpisut, P., Kloda, A. & Martinac, B. (2002). Open channel structure of MscL and the gating mechanism of mechanosensitive channels. *Nature* **418**, 942–948.

Persson, M., Harbridge, J. R., Hammerström, P., Mitri, R., Mårtensson, L.-G., Carlsson, U., Eaton, G. R. & Eaton, S. S. (2001). Comparison of electron paramagnetic resonance methods to determine distances between spin labels on human carbonic anhydrase II. *Biophysical Journal* **80**, 2886–2897.

Pfannebecker, V., Klos, H., Hubrich, M., Volkmer, T., Heuer, A., Wiesner, U. & Spiess, H. W. (1996). Determination of end-to-end distances in oligomers by pulsed EPR. *Journal of Physical Chemistry* **100**, 13428–13432.

Piton, N., Schiemann, O., Mu, Y., Stock, G., Prisner, T. F. & Engels, J. W. (2005). Synthesis of spin-labeled RNAS for long range distance measurements by PELDOR. *Nucleosides, Nucleotides, and Nucleic Acids* **24**, 771–775.

Piton, N., Mu, Y., Stock, G., Prisner, T. F., Schiemann, O. & Engels, J. W. (2007). Base specific spin-labeling of RNA for structure determination. *Nucleic Acids Research* **35**, 3128–3143.

Polyhach, Y., Godt, A., Bauer, C. & Jeschke, G. (2007). Spin pair geometry revealed by high-field DEER in the presence of conformational distributions. *Journal of Magnetic Resonance* **185**, 118–129.

Pornsuwan, S., Bird, G., Schafmeister, C. E. & Saxena, S. (2006). Flexibility and lengths of bis-peptide nanostructures by electron spin resonance. *Journal of the American Chemical Society* **128**, 3876–3877.

Prisner, T. F., Rohrer, M. & MacMillan, F. (2001). Pulsed EPR spectroscopy: biological applications. *Annual Review of Physical Chemistry* **52**, 279–313.

Prisner, T. F. (1997). Pulsed high-frequency/high-field EPR. *Advances in Magnetic and Optical Resonance* **20**, 245–299.

Prisner, T. F., Est, A. V. D., Bittl, R., Lubitz, W., Stehlik, D. & Möbius, K. (1995). Time-resolved W-band (95 GHz) EPR spectroscopy of Zn-substituted reaction centers of *Rhodobacter sphaeroides* R-26. *Chemical Physics* **194**, 361–370.

Qin, P. Z., Butcher, S. E., Feigon, J. & Hubbell, W. L. (2001). Quantitative analysis of the isolated GAAA tetraloop/receptor interaction in solution: a site-directed spin labeling study. *Biochemistry* **40**, 6929–6936.

Qin, P. Z. & Dieckmann, T. (2004). Application of NMR and EPR methods to the study of RNA. *Current Opinion in Structural Biology* **14**, 350–359.

Qin, P. Z., Hideg, K., Feigon, J. & Hubbell, W. L. (2003). Monitoring RNA base structure and dynamics using site-directed spin labeling. *Biochemistry* **42**, 6772–6783.

Rabenstein, M. D. & Shin, Y.-K. (1995). Determination of the distance between two spin labels attached to a macromolecule. *Proceedings of the National Academy of Sciences USA* **92**, 8239–8243.

Raitsimring, A., Crepeau, R. H. & Freed, J. H. (1995). Nuclear modulation effects in '2 + 1' electron spin-echo correlation spectroscopy. *Journal of Chemical Physics* **102**, 8746–8762.

Raitsimring, A., Peisach, J., Lee, H. C. & Chen, X. (1992). Measurement of distance distributions between spin labels in spin-labeled hemoglobin using an electron spin echo methods. *Journal of Physical Chemistry* **96**, 3526–3531.

Rakowsky, M. H., More, K. M., Kulikov, A. V., Eaton, G. R. & Eaton, S. S. (1995). Time-domain electron paramagnetic resonance as a probe of electron–electron spin–spin interaction in spin-labeled low-spin iron porphyrins. *Journal of the American Chemical Society* **117**, 2049–2057.

Ramos, A. & Varani, G. (1998). A new method to detect long-range protein-RNA contacts: NMR detection of electron–proton relaxation induced by nitroxide spin-labeled RNA. *Journal of the American Chemical Society* **120**, 10992–10993.

Rassat, A. & Rey, P. (1967). Nitroxides, XXIII. Préparation d'aminoacides radicalaires et de leurs sels complexes. *Bullétin de la Société Chimique de France*, 815–817.

Robinson, B. H. & Drobny, G. P. (1995). Site-specific dynamics in DNA: theory. *Annual Review of Biophysics and Biomolecular Structure* **24**, 523–549.

Robinson, B. H., Mailer, C. & Drobny, G. (1997). Site-specific dynamics in DNA: experiments. *Annual Review of Biophysics and Biomolecular Structure* **26**, 629–658.

Sale, K., Faulon, J.-L., Gray, G. A., Schoeniger, J. S. & Young, M. M. (2004). Optimal bundling of transmembrane helices sparse distance constraints. *Protein Science* **13**, 2613–2627.

Sale, K., Song, L., Liu, Y.-S., Perozo, E. & Fajer, P. (2005). Explicit treatment of spin labels in modeling of distance constraints from dipolar EPR and DEER. *Journal of the American Chemical Society* **127**, 9334–9335.

Salikhov, K. M., Bock, C. H. & Stehlik, D. (1990). Time development of electron spin polarization in magnetically coupled, spin correlated pairs. *Applied Magnetic Resonance* **1**, 195–211.

Salikhov, K. M., Dzuba, S. A. & Raitsimring, A. M. (1981). The theory of electron spin-echo signal decay resulting from dipole–dipole interactions between paramagnetic centers in solids. *Journal of Magnetic Resonance* **42**, 255–276.

Salikhov, K. M., Semenov, A. G. & Tsvetkov, Y. D. (1976). *Electron Spin Echo and Its Applications*. Nauka: Novosibirsk.

Salnikov, E. S., Erilov, D. A., Milov, A. D., Tsvetkov, Y. D., Peggion, C., Formaggio, F., Toniolo, C., Raap, J. & Dzuba, S. A. (2006). Location and aggregation of the spin-labeled peptide trichogin GA IV in a phospholipid membrane as revealed by pulsed EPR. *Biophysical Journal* **91**, 1532–1540.

Santabarbara, S., Kuprov, I., Fairclough, W. V., Purton, S., Hore, P. J., Heathcote, P. & Evans, M. C. W. (2005). Bidirectional electron transfer in photosystem I: determination of two distances between P_{700}^{+} and A_{1}^{-} in spin-correlated radical pairs. *Biochemistry* **44**, 2119–2128.

Saxena, S. & Freed, J. H. (1996). Double quantum two-dimensional Fourier transform electron spin resonance: distance measurements. *Chemical Physics Letters* **251**, 102–110.

Saxena, S. & Freed, J. H. (1997). Theory of double quantum two-dimensional electron spin resonance with application to distance measurements. *Journal of Chemical Physics* **107**, 1317–1340.

Schiemann, O., Piton, N., Mu, Y., Stock, G., Engels, J. W. & Prisner, T. F. (2004). A PELDOR-based nanometer distance ruler for oligonucleotides. *Journal of the American Chemical Society* **126**, 5722–5729.

Schiemann, O., Piton, N., Plackmeyer, J., Bode, B. E., Prisner, T. F. & Engels, J. W. (2007). Spin-Labeling of RNA/DNA with TPA and Nanometer Distance Measurements by PELDOR. *Nature Protocols* **2**, 904–923.

Schiemann, O., Weber, A., Edwards, T. E., Prisner, T. F. & Sigurdsson, S. T. (2003). Nanometer distance measurements on RNA using PELDOR. *Journal of the American Chemical Society* **125**, 3434–3435.

Scholes, C. P., Janakiraman, R., Taylor, H. & King, T. E. (1984). Temperature dependence of the electron spin-lattice relaxation rate from pulsed EPR of Cu_A and heme *a* in cytochrome *c* oxidase. *Biophysical Journal* **45**, 1027–1030.

Schweiger, A. & Jeschke, G. (2001). *Principles of Pulse Electron Paramagnetic Resonance*. Oxford: Oxford University Press.

Sharp, R., Lohr, L. & Miller, J. (2001). Paramagnetic NMR relaxation enhancement: recent advances in theory. *Progress in Nuclear Magnetic Resonance Spectroscopy* **38**, 115–158.

Shigemori, K., Hara, H., Kawamori, A. & Akabori, K. (1998). Determination of distances from tyrosine D to Q_A and chlorophyll Z in photosystem II studied by '2 + 1' pulsed EPR. *Biochimica et Biophysica Acta* **1363**, 187–198.

Slichter, C. P. (1980). *Principles of Magnetic Resonance*. Berlin: Springer Verlag.

Snyder, S. W. & Thurnauer, M. C. (1993). Electron spin polarization in photosynthetic reaction centers. In *The Photosynthetic Reaction Center*, vol. 2 (eds. J. Deisenhofer & J. R. Norris), pp. 285–330. New York: Academic Press.

Spaltenstein, A., Robinson, B. H. & Hopkins, P. B. (1989). DNA structural data from a dynamics probe. The dynamic signatures of single-stranded, hairpin-looped and duplex forms of DNA are distinguishable. *Journal of the American Chemical Society* **111**, 2303–2305.

Sprinzl, M., Krämer, E. & Stehlik, D. (1974). On the structure of phenylalanine tRNA from yeast. Spin label studies. *European Journal of Biochemistry* **49**, 595–605.

Stehlik, D. & Möbius, K. (1997). New EPR methods for investigating photoprocesses with paramagnetic intermediates. *Annual Review of Physical Chemistry* **48**, 745–784.

Steigmiller, S., Börsch, M., Gräber, P. & Huber, M. (2005). Distances between the b-subunits in the tether domain of F_0F_1-ATP synthase from *E. coli*. *Biochimica et Biophysica Acta* **1708**, 143–153.

Steinhoff, H.-J. (2004). Inter- and intra-molecular distances determined by EPR spectroscopy and site-directed spin labeling reveal protein–protein and protein–oligonucleotide interaction. *Biological Chemistry* **385**, 913–920.

Steinhoff, H.-J., Radziwill, N., Thevis, W., Lenz, V., Brandenburg, D., Antson, A., Dodson, G. & Wollmer, A. (1997). Determination of interspin distances between spin labels attached to insulin: comparison of electron paramagnetic resonance data with the X-ray structure. *Biophysical Journal* **73**, 3287–3298.

Strube, T., Schiemann, O., MacMillan, F., Prisner, T. F. & Engels, J. W. (2001). A new facial method for spin-labeling of oligonucleotides. *Nucleosides, Nucleotides, and Nucleic Acids* **20**, 1271–1274.

Stubbe, J., Nocera, D. G., Yee, C. S. & Chang, M. C. Y. (2003). Radical initiation in the class I ribonucleotide reductase: long-range proton-coupled electron transfer. *Chemical Reviews* **103**, 2167–2201.

Sun, J. J., Voss, J., Hubbell, W. L. & Kaback, H. R. (1999). Proximity between periplasmic loops in the lactose permease of *Escherichia coli* as determined by site-directed spin labeling. *Biochemistry* **38**, 3100–3105.

Thurnauer, M. C. & Clark, C. (1984). Electron spin echo envelope modulation of the transient EPR signals observed in photosynthetic algae and chloroplasts. *Photochemistry and Photobiology* **40**, 381–386.

Timmel, C. R., Fursman, C. E., Hoff, A. J. & Hore, P. J. (1998). Spin-correlated radical pairs: microwave pulse effects on lifetimes, electron spin echo envelope modulations, and optimum conditions for detection by electron spin echo spectroscopy. *Chemical Physics* **226**, 271–283.

Tjandra, N., Grzesiek, S. & Bax, A. (1996). Magnetic field dependence of nitrogen-proton J splittings in ^{15}N-enriched human ubiquitin resulting from relaxation interference and residual dipolar coupling. *Journal of the American Chemical Society* **118**, 6264–6272.

Tocilj, A., Schluenzen, F., Hansen, H. A., Bashan, A., Janell, D., Gluehmann, M., Bartels, H., Harms, J., Agmon, I., Franceschi, F. & Yonath, A. (1999). The small ribosomal subunit from *Thermus thermophilus* at 4·5 Å resolution: pattern fittings and the identification of a functional site. *Proceedings of the National Academy of Sciences USA* **96**, 14252–14257.

Tolman, J. R., Flanagan, J. M., Kennedy, M. A. & Prestegard, J. H. (1995). Nuclear magnetic dipole interactions in field-oriented proteins: information for structure determination in solution. *Proceedings of the National Academy of Sciences USA* **92**, 9279–9283.

Tonaka, M., Kawamori, A., Hara, H. & Astashkin, A. V. (2000). Three dimensional structure of electron transfer components in photosystem II: '2+1' ESE of chlorophyll Z and tyrosin D. *Applied Magnetic Resonance* **19**, 141–150.

Ubbink, M., Worrall, J. A. R., Canters, G. W., Groenen, E. J. J. & Huber, M. (2002). Paramagnetic resonance of biological metal centers. *Annual Review of Biophysics and Biomolecular Structure* **31**, 393–422.

Un, S., Brunel, L.-C., Brill, T. M., Zimmermann, J.-L. & Rutherford, A. W. (1994). Angular orientation of the stable tyrosyl radical within photosystem II by high-field 245 GHz electron paramagnetic resonance. *Proceedings of the National Academy of Sciences USA* **91**, 5262–5266.

Verma, S. & Eckstein, F. (1998). Modified oligonucleotides: synthesis and strategy for users. *Annual Reviews of Biochemistry* **67**, 99–134.

Voss, J., Hubbell, W. L. & Kaback, H. R. (1995a). Distance determination in proteins using designed metal ion binding sites and site-directed sping labeling: application to the lactose permease of *Escherichia coli*. *Proceedings of the National Academy of Sciences USA* **92**, 12300–12303.

Voss, J., Salwinski, L., Kaback, H. R. & Hubbell, W. L. (1995b). A method for distance determination in proteins using a designed metal ion binding site and site-directed spin labeling: evaluation with T4 lysozyme. *Proceedings of the National Academy of Sciences USA* **92**, 12295–12299.

Voss, J., Hubbell, W. L. & Kaback, H. R. (1998). Helix packing in the lactose permease determined by metal-nitroxide interaction. *Biochemistry* **37**, 211–216.

Weber, A., Schiemann, O., Bode, B. & Prisner, T. (2002). PELDOR at S- and X-band frequencies and the separation of exchange coupling form dipolar coupling. *Journal of Magnetic Resonance* **157**, 277–285.

Wegener, A.-A., Klare, J. P., Engelhard, M. & Steinhoff, H.-J. (2001). Structural insights into the early steps of receptor-transducer signal transfer in archael phototaxis. *European Molecular Biology Journal* **20**, 5312–5319.

Wüthrich, K. (1986). *NMR of Proteins and Nucleic Acids*. New York: John Wiley & Sons.

Xu, Q., Ellena, J. F., Kim, M. & Cafiso, D. S. (2006). Substrate-dependent unfolding of the energy coupling motif of a membrane transport protein determined by double electron-electron resonance. *Biochemistry* **45**, 10847–10854.

Yang, K., Farrens, D. L., Altenbach, C., Farahbakhsh, Z. T., Hubbell, W. L. & Khorana, H. G. (1996). Structure and function in rhodopsin. Cysteines 65 and

316 are in proximity in a rhodopsin mutant as indicated by disulfide formation and interactions between attached spin labels. *Biochemistry* **35**, 14040–14046.

Yoshii, T., Hara, H., Kawamori, A., Akabori, K., Iwaki, M. & Itoh, S. (1999a). ESEEM study of the location of spin polarized chlorophyll-quinone radical pair in membrane-oriented spinach photosystem I and II complexes. *Applied Magnetic Resonance* **16**, 565–580.

Yoshii, T., Kawamori, A., Tonaka, M. & Akabori, K. (1999b). Relative positions of electron transfer components in photosystem II studied by '2+1' pulsed electron paramagnetic resonance: Y_D and Q_A. *Biochimica et Biophysica Acta* **1413**, 43–49.

Yusupov, M., Yusupova, G., Baucom, A., Lieberman, K., Earnest, T. N., Cate, J. H. & Noller, H. F. (2001). Crystal structure of the ribosome at 5·5 Å resolution. *Science* **292**, 883–896.

Zech, S. G., Kurreck, J., Eckert, H.-J., Renger, G., Lubitz, W. & Bittl, R. (1997). Pulsed EPR measurement of the distance between $P_{680}^{+\bullet}$ and $Q_A^{-\bullet}$ in photosystem II. *Federation of European Biochemical Societies Letters* **414**, 454–456.

Zech, S. G., Kurreck, J., Renger, G., Lubitz, W. & Bittl, R. (1999). Determination of the distance between $Y_Z^{ox\bullet}$ and $Q_A^{-\bullet}$ in photosystem II by pulsed EPR spectroscopy on light-induced radical pairs. *Federation of European Biochemical Societies Letters* **442**, 79–82.

Zhidomirov, G. M. & Salikhov, K. M. (1969). Contribution to the theory of spectral diffusion in magnetically diluted solids. *Soviet Physics JETP* **29**, 1037–224.

Zhou, Z., DeSensi, S. C., Stein, R. A., Brandond, S., Dixit, M., McArdle, E. J., Warren, E. M., Kroh, H. K., Song, L., Cobb, C. E., Hustedt, E. J. & Beth, A. H. (2005). Solution structure of the cytoplasmic domain of erythrocyte membrane band 3 determined by site-directed spin labeling. *Biochemistry* **44**, 15115–15128.

Zouni, A., Witt, H. T., Kern, J., Fromme, P., Krauß, N., Saenger, W. & Orth, P. (2001). Crystal structure of photosystem II from *Synechococcus elongatus* at 3·8 Å resolution. *Nature* **409**, 739–743.

Zwanenburg, G. & Hore, P. J. (1993). EPR of spin-correlated radical pairs. Analytical treatment of selective excitation including zero-quantum coherence. *Chemical Physics Letters* **203**, 65–74.